NEUROSCIENCE

Sex differences in neural projections of fear memory processing in mice and humans

Antonio Florido[1,2], Eric R. Velasco[1]†, Leire R. Romero[1], Neha Acharya[1], Ignacio J. Marin Blasco[1], Jaime F. Nabás[1], Laura Perez-Caballero[1,2], Guadalupe Rivero[3,4,5], Estíbaliz Olabarrieta[3,4], Amaia Nuñez-delMoral[3,4], Jose A. González-Parra[6], Daniel Porta-Casteràs[4,7,8,9], Marta Cano[4,7], Trevor Steward[10,11], Monica S. Antony[12], Narcís Cardoner[4,7,8,9], Rafael Torrubia[13], Alexander C. Jackson[12,14], Miquel A. Fullana[4,15], Raül Andero[1,2,4,16,17]*

It remains unexplored in the field of fear memory whether functional neuronal connectivity between two brain areas is necessary for one sex but not the other. Here, we show that chemogenetic silencing of centromedial (CeM)–*Tac2* fibers in the lateral posterior BNST (BNSTpl) decreased fear memory consolidation in male mice but not females. Optogenetic excitation of CeM-*Tac2* fibers in the BNSTpl exhibited enhanced inhibitory postsynaptic currents in males compared to females. In vivo calcium imaging analysis revealed a sex-dimorphic fear memory engram in the BNSTpl. Furthermore, in humans, the single-nucleotide polymorphism (SNP) in the Tac2 receptor (rs2765) (*TAC3R*) decreased CeM-BNST connectivity in a fear task, impaired fear memory consolidation, and increased the expression of the *TAC3R* mRNA in AA-carrier men but not in women. These sex differences in critical neuronal circuits underlying fear memory formation may be relevant to human neuropsychiatric disorders with fear memory alterations such as posttraumatic stress disorder.

INTRODUCTION

Neuronal circuits play an essential role in encoding, storing, and retrieving environmental threat-predicting cues, forming the basis of what is known as fear memory (*1*, *2*). These memories are not only crucial for decision-making but also trigger automatic responses to threats (*3*). This neurobiological understanding, enriched by comparative studies in humans and mice, who share key neural aspects of fear response (*4*), is crucial for advancing the treatment of fear-based disorders (*4*, *5*).

Our study builds upon seminal work that uncovered the role of the tachykinin 2 (Tac2) pathway in the central amygdala (CeA) in modulating fear memory consolidation. This prior research revealed a sex-specific effect in which CeA-*Tac2* antagonism and its pharmacogenetic temporal inhibition impaired fear memory in male mice but, unexpectedly, enhanced it in female mice. These findings, alongside the identification of CeA-testosterone and CeA-estradiol, in addition to Akt/GSK3β/β-catenin signaling, as mediators of this sex-differential regulation, set a precedent for further exploration into the molecular mechanisms of fear memory (*6*).

Notwithstanding this prior work, the field is still confronting the challenge of underrepresentation of female samples in basic science research, despite their higher prevalence in stress and fear-based disorders (*7*, *8*). This gap is partly due to presumed variability related to the estrous cycle among other factors (*9*, *10*). Although sex differences in fear memory processing have been established at the molecular and behavioral levels in both rodents and humans (*3*, *11*), comparable response variability between female and male rodents remains (*12*). This paradox highlights the need for deeper insights into the sex-specific neurocircuitry involved in fear memory formation.

In this context, our study delves into an aspect of memory formation: the necessity of connectivity between specific brain regions for memory formation and whether this requirement is sex specific. We hypothesize that the chemogenetic silencing of the centromedial amygdala, a subregion of CeA (CeM)-*Tac2* fibers in the lateral posterior region of the bed nucleus of the stria terminalis (BNSTpl or STPL), affects fear memory consolidation differently in male and female mice. We anticipate that optogenetic stimulation will reveal disparate inhibitory connectivity of CeM-*Tac2* fibers in the BNSTpl between sexes. Furthermore, in vivo calcium imaging will potentially uncover sex-dimorphic engrams of fear memory within the BNSTpl. Extending our investigation to healthy humans, we aim to understand how a single-nucleotide polymorphism (SNP) in the Tac2 receptor (rs2765) (*TAC3R*) affects CeM-BNST connectivity during a fear task and its subsequent impact on fear memory consolidation and *TAC3R* mRNA expression, especially in AA-carrier men compared to women. This research could provide critical insights into the neuropathological underpinnings of mental disorders characterized by memory alterations, such as posttraumatic stress disorder (PTSD).

[1]Institut de Neurociències, Universitat Autònoma de Barcelona, Cerdanyola del Vallès, Barcelona, Spain. [2]Departament de Psicobiologia i de Metodologia de les Ciències de la Salut, Universitat Autònoma de Barcelona, Cerdanyola del Vallès, Barcelona, Spain. [3]Department of Pharmacology, University of the Basque Country, UPV/EHU, Leioa, Spain. [4]Centro de Investigación Biomédica en Red de Salud Mental (CIBERSAM), Madrid, Spain. [5]Biobizkaia Health Research Institute, Barakaldo, Spain. [6]IMIM-Hospital del Mar Medical Research Institute, Cell-Type Mechanisms in Normal and Pathological Behavior, Barcelona, Spain. [7]Sant Pau Mental Health Research Group, Institut de Recerca Sant Pau (IR SANT PAU), Barcelona, Spain. [8]Mental Health Department, Unitat de Neurociència Traslacional, Parc Tauli University Hospital, Institut d'Investigació i Innovació Sanitària Parc Taulí (I3PT), Barcelona, Spain. [9]Department of Psychiatry and Forensic Medicine, School of Medicine Bellaterra, Universitat Autònoma de Barcelona, Barcelona, Spain. [10]Melbourne School of Psychological Sciences, The University of Melbourne, Parkville, Victoria, Australia. [11]Department of Psychiatry, The University of Melbourne, Parkville, Victoria, Australia. [12]Department of Physiology and Neurobiology, University of Connecticut, Storrs, CT, USA. [13]Unitat de Psicologia Mèdica, Departament de Psiquiatria i Medicina Legal and Institut de Neurociències, Universitat Autònoma de Barcelona, Bellaterra, Barcelona, Spain. [14]The Institute for the Brain and Cognitive Sciences (IBACS), Storrs, CT, USA. [15]Institut d'Investigacions Biomèdiques August Pi i Sunyer (IDIBAPS), Adult Psychiatry and Psychology Department, Institute of Neurosciences, Hospital Clinic, Barcelona, Spain. [16]Unitat de Neurociència Traslacional, Parc Taulí Hospital Universitari, Institut d'Investigació i Innovació Parc Taulí (I3PT), Sabadell, Spain. [17]ICREA, Barcelona, Spain.

*Corresponding author. Email: raul.andero@uab.cat

†Present address: Department of Radiology, Institut Català de la Salut (ICS), Hospital Universitari Vall d'Hebron, Barcelona, Spain.

RESULTS

CeM-*Tac2* connectivity

Silencing CeM-*Tac2* neurons has been shown to decrease fear memory consolidation in males and increase it in females, in a manner dependent on the hormonal state of the animal (*6*). To investigate the role of these structures on other brain regions involved in memory and conditioned fear, we performed an anatomical study of projections in males and females followed by a functional analysis based on cFos expression in mCherry-positive areas. First, we conducted anatomical tracing of projection fibers from CeM-*Tac2* neurons to other brain regions. We injected AAV8-hSyn-DIO-hM4D(Gi)-mCherry in *Tac2*-Cre$^{-/+}$ across both female and male mice and found statistically significant sex differences in the integrated density of mCherry expression in the BNST (Fig. 1, A to D). Males exhibited higher fluorescence density in BNST subregions [STMPI (P = 0.021), STMPL (P = 0.021), and STPL (P = 0.021)], while females showed higher fluorescence density in the lateral periaqueductal gray region [LPAG (P = 0.003) and VLPAG (P = 0.033)] (Fig. 1, B to D, and table S1).

We further used the anterograde tracer H129ΔTK-TT targeted to CeM-*Tac2* neurons (Fig. 1E). The expression of tdTomato (tdT) 72 hours postinfection (*13*) revealed a higher fluorescence density associated with this reporter in males in the prefrontal cortex

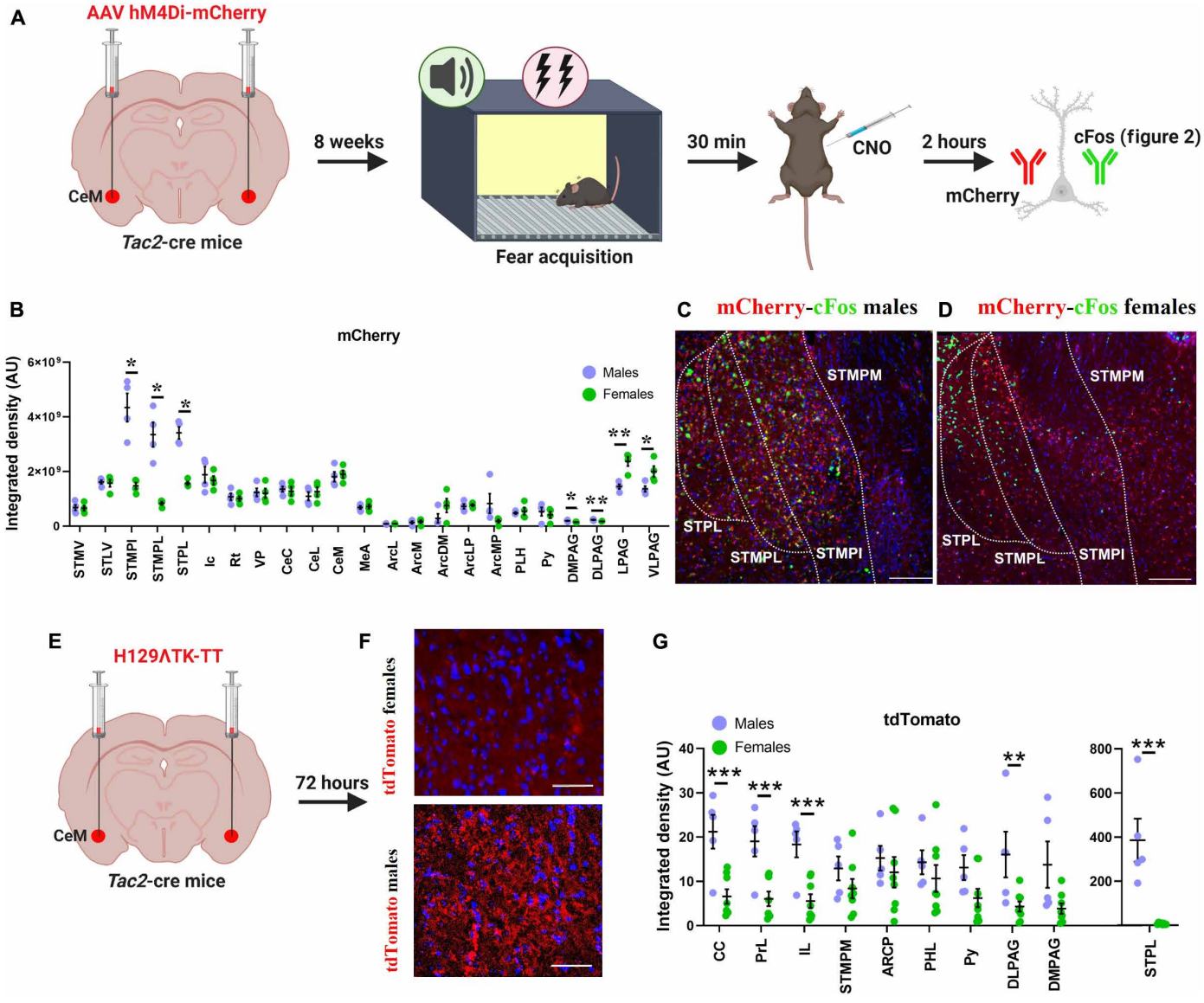

Fig. 1. Males exhibit denser projections of CeM-*Tac2* to the lateral posterior BNST. (**A**) Schematic timeline of the procedure. Created with BioRender.com. (**B**) Distribution of mCherry expression across the mouse brain in males and females following infection of CeM-*Tac2* neurons with hM4Di-mCherry in cFos expressing regions. (**C**) Representative confocal image of the lateral posterior BNST (or STPL) in a male mouse infected with hM4Di-mCherry in CeM-*Tac2* neurons. (**D**) Representative confocal image of the lateral posterior BNST in a female mouse infected with hM4Di-mCherry in CeM-*Tac2* neurons. (**E**) Schematic depiction of the H129ΔTK-TT inoculation in the CeM. Created with BioRender.com. (**F**) Representative confocal image showing tdTomato (tdT) expression in the lateral posterior BNST of female and male mice. (**G**) Distribution of tdT expression in target areas from CeM-*Tac2* neurons in male and female mice. Data were analyzed using *t* test or Mann-Whitney's *U*. **P* < 0.05, ***P* < 0.01, and ****P* < 0.001. AU, arbitrary units.

[Cg ($P = 0.013$), PrL ($P = 0.013$), and IL ($P = 0.013$)], the periaqueductal gray matter [DLPAG ($P = 0.018$)] and the BNSTpl [STPL ($P = 0.003$)] but not in the medial STPM region ($P = 0.219$) (Fig. 1, E to G). These two anatomical studies highlight sex-specific differences in the distribution of CeM-*Tac2* neuron fibers, affecting critical regions involved in conditioned fear processing, such as the BNSTpl. These findings uncover novel sex differences in neural projections of fear.

Correlational analysis of cFos expression

In the context of fear memory consolidation [2 hours post–clozapine-*N*-oxide (CNO), 2.5 hours post-fear acquisition (FA)], *Tac2*-Cre$^{-/+}$ males exhibited heightened cFos counts in the arcuate nucleus of the hypothalamus [ArcM ($P = 0.021$), ArcMP ($P = 0.021$), and ArcDM ($P = 0.011$)], the pyramidal layer of the hippocampus [Py ($P = 0.033$)], the BNST [STMPI ($P = 0.021$), STMPL ($P = 0.008$), and STPL ($P = 0.021$)], and the periaqueductal gray [DLPAG ($P = 0.043$), LPAG ($P < 0.001$), and VLPAG ($P = 0.032$)] while displaying reduced counts in the CeA [CeM ($P = 0.019$) and CeL ($P = 0.023$)] compared to *Tac2*-Cre$^{-/-}$ male mice. CeM-*Tac2* silencing in *Tac2*-Cre$^{-/+}$ female mice resulted in a decreased cFos-positive cell count in CeM ($P = 0.002$), CeL ($P = 0.021$), ArcM ($P = 0.016$), ArcMP ($P = 0.034$), and ArcDM ($P = 0.005$) compared to *Tac2*-Cre$^{-/-}$ female mice (fig. S1).

To assess the impact of silencing *Tac2* neurons in CeM on long-range functional connections between brain regions during fear memory consolidation, we conducted a correlational analysis of cFos expression in both sexes using *Tac2*-Cre$^{-/-}$ and *Tac2*-Cre$^{-/+}$ mice. Our analysis revealed significant negative Pearson's correlations between the cFos cell count in CeM and BNST regions in *Tac2*-Cre$^{-/-}$ male mice: STMPI ($P = 0.032$), STMPL ($P = 0.038$), and STPL ($P = 0.027$), among other areas (Fig. 2, A to H). Notably, these correlations were not statistically significant in *Tac2*-Cre$^{-/+}$ male mice [STMPI ($P = 0.898$), STMPL ($P = 0.129$), and STPL ($P = 0.165$)] or in females, irrespective of genotype [*Tac2*-Cre$^{-/+}$: STMPI ($P = 0.895$), STMPL ($P = 0.194$), and STPL ($P = 0.602$); *Tac2*-Cre$^{-/-}$: STMPI ($P = 0.659$), STMPL ($P = 0.926$), and STPL ($P = 0.767$)] (figs. S2 and S3). These data highlight differences in *Tac2*-mediated neuronal activity between males and females during fear memory consolidation.

Chemogenetic silencing of CeM-*Tac2* neurons projecting to the BNSTpl

Given the dissociation observed between anatomical and functional connectivity, our study aimed to investigate whether these sex-specific connections between *Tac2* neurons in the CeM and the BNSTpl differentially regulate conditioned fear responses. To address

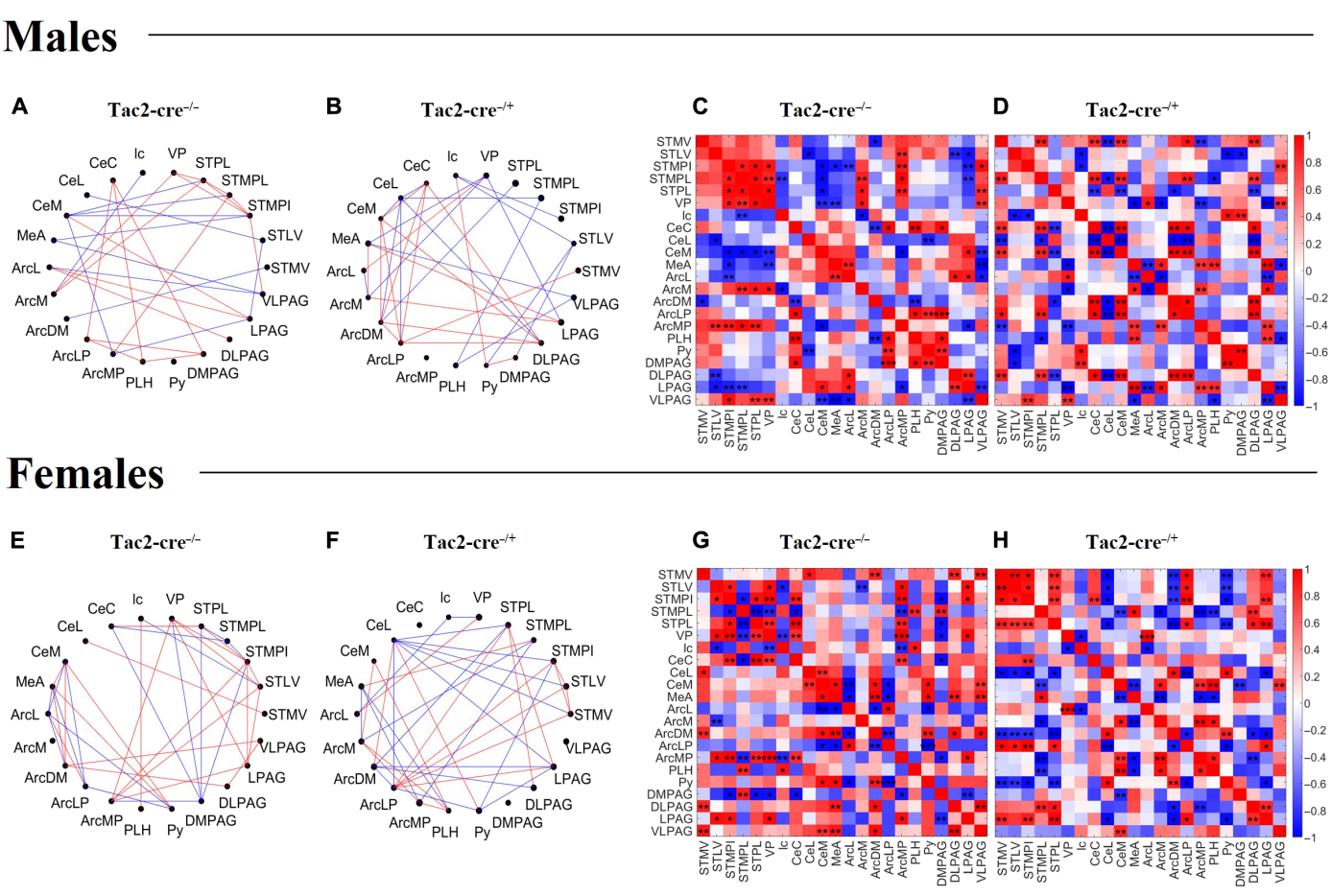

Fig. 2. cFos correlational analyses upon CeM-*Tac2* temporal inhibition after FA. (**A**) High and significant correlations of cFos expression between areas in *Tac2*-Cre$^{-/-}$ males and (**B**) *Tac2*-Cre$^{-/+}$ males. (**C**) Heatmaps representing Pearson correlation coefficients of cFos expression between areas in *Tac2*-Cre$^{-/-}$ males and (**D**) *Tac2*-Cre$^{-/+}$ males. (**E**) High and significant correlations of cFos expression between areas in *Tac2*-Cre$^{-/-}$ females and (**F**) *Tac2*-Cre$^{-/+}$ females. (**G**) Heatmaps representing Pearson correlation coefficients of cFos expression between areas in *Tac2*-Cre$^{-/-}$ females and (**H**) *Tac2*-Cre$^{-/+}$ females. Data were analyzed using Pearson's *R* coefficient. *$P < 0.05$, **$P < 0.01$, and ***$P < 0.001$.

this question, male and female *Tac2*-Cre$^{-/-}$ and *Tac2*-Cre$^{-/+}$ mice, following the injection of AAV8-DIO-hM4Di-mCherry in CeM, underwent a conditioned fear task (Fig. 3A). CNO was delivered through a cannula in the BNSTpl to inhibit the terminals of *Tac2* neurons projecting from CeM. *Tac2*-Cre$^{-/+}$ male mice that received local CNO exhibited less freezing in response to the tone compared to *Tac2*-Cre$^{-/-}$ males (Fig. 3, B and C). Females were unaffected by the treatment, with *Tac2*-Cre$^{-/-}$ and *Tac2*-Cre$^{-/+}$ female mice showing similar freezing rates in response to the tone during the fear expression (FE) test (Fig. 3, D and E, and fig. S4).

CeM-*Tac2* afferents to the BNSTpl and synaptic connectivity in vitro

Owing to the GABAergic nature of CeM-*Tac2* neurons (*6*, *14*), we examined whether inhibitory synaptic connectivity with BNST neurons exhibited any sexual dimorphism. Given a denser projection of *Tac2* fibers in males than in females, we hypothesized increased postsynaptic inhibitory connectivity in males after stimulation of CeM-*Tac2* neurons. To this end, we expressed ChR2 in CeM-*Tac2* neurons of both male and proestrus female *Tac2*-Cre$^{-/+}$ mice and carried out whole-cell voltage-clamp recordings of optically evoked inhibitory postsynaptic currents (oIPSCs) from BNST neurons (Fig. 3, F to M). We confirmed accurate targeting of the CeM in *Tac2*-Cre$^{-/+}$ mice (Fig. 3G) and mapped the anatomical location of recorded neurons within the region of the BNSTpl between the fornix and internal capsule (in coronal slices between approximately −0.10 and −0.22 mm from bregma; Fig. 3, H and I). We then examined both the rate of connectivity and amplitude of oIPSCs (Fig. 3, J to M). In both males and females, we found that neurons that exhibited oIPSCs in response to blue light were concentrated in the region close to the internal capsule (Fig. 3, H and I). The comparison of proportions of connected cells between male and female mice revealed a significantly higher proportion of synaptically connected neurons in males compared to female mice ($P = 0.043$) (Fig. 3J). While the amplitude of oIPSCs was variable in both males and females, the mean amplitude of oIPSCs (including both responders and nonresponders) in BNST neurons was higher in males than in females ($P = 0.049$) (Fig. 3K). In comparing the oIPSC amplitude of only responders, the average difference was not significant ($P = 0.229$) (Fig. 3L). These data suggest a modest sexual dimorphism in inhibitory synaptic connectivity between CeM-*Tac2* neurons and BNST neurons in vitro.

In vivo calcium imaging in freely moving mice

Having demonstrated the functional involvement of the BNSTpl in *Tac2*-regulated fear memory consolidation in males, but not in females, our next aim was to establish the physiological effect that this manipulation has on the formation of memory engrams in the BNSTpl (Fig. 4A). There were no differences in freezing or shock reactivity during FA between male and female *Tac2*-Cre$^{-/-}$ and *Tac2*-Cre$^{-/+}$ mice, and repeated measures analysis of variance (ANOVA) revealed a significant sex-by-genotype interaction in tone-induced freezing [$F_{(1,12)} = 30.576$, $P < 0.001$; for males, main effect genotype: $F_{(1,6)}$=17.155, $P = 0.006$; for females, main effect genotype: $F_{(1,6)}$=13.421, $P = 0.011$] (Fig. 4, B and C, and fig. S5A).

In males, the fluorescence emitted by GCaMP6f was increased in *Tac2*-Cre$^{-/+}$ compared to *Tac2*-Cre$^{-/-}$ mice during the pre–conditioned stimulus (CS) ($P < 0.000$), CS ($P < 0.0000$), and intertrial intervals (ITIs) ($P < 0.0000$) (Fig. 4, D to F, and fig. S5, B to D). In females, however, this fluorescence increased in *Tac2*-Cre$^{-/+}$ mice during the preCS ($P = 0.018$) but not during the ITI or in the presence of the tone (Fig. 4, G to I). Furthermore, the analysis of freezing correlation with each neuron of each animal revealed that silencing *Tac2* neurons in CeM decreased the proportion of BNST neurons significantly correlated with freezing ($P = 0.029$) (Fig. 4J), while in females, these proportions were unaffected by the treatment ($P = 0.112$) (Fig. 4K). These data highlight the reduction in functional relationships between the BNSTpl and freezing in males following the silencing of CeM-*Tac2* neurons.

CeM-BNST connectivity and rs2765 in the *TAC3R* gene

Given the notable differences observed in *Tac2*-associated connectivity between CeM and the BNSTpl in mice, we investigated the functional connectivity of this pathway in human fear processing using data from the Human Connectome Project (HCP) (Fig. 5A). According to these data, a previous study identified a significant association between the SNP rs2765 within the *TAC3R* gene (encoding Nk3R) and learning and memory in aged humans (*15*). Furthermore, it has been reported that the activation or inhibition of the *Tac2* and Nk3R has opposite effects depending on sex in fear of memory consolidation in mice (*6*).

Genotype by sex frequencies and participants´ characteristics

Because the GG genotype had a much lower frequency compared to the rest, AG and GG participants were combined into a G-carrier genotype group. Participants were clustered according to their genotype (AA or GA/GG) and sex, resulting in 205 women in the AA group, 390 women in the GA/GG group, 183 men in the AA group, and 276 men in the GA/GG group (table S2).

Negative connectivity between CeM and BNST

Men participants in the AA group exhibited significantly higher negative connectivity between the left CeM and the right BNST compared to men participants in the GA/GG group ($P_{FWE} = 0.025$; $t = 2.91$; $x, y, z = 8, 6, 0$) (Fig. 5, A to C). However, no significant findings were observed when assessing women participants (Fig. 5D).

Men carrying the GG/GC allele show a higher vulnerability to psychopathology

Furthermore, men participants in the AA group, in contrast to those in the GA/GG group, demonstrated more favorable mental health outcomes across various psychological constructs, encompassing perceived stress ($P = 0.009$) and hostility ($P = 0.044$) and neuroticism ($P = 0.044$; table S3 and fig. S6). Notably, the adult self-report indicated increased internalization ($P = 0.044$), particularly highlighting elevated levels of anxiety and depression ($P = 0.044$), thought problems ($P = 0.044$), and attention problems ($P = 0.044$), with no significant effect on the externalization scale ($P = 0.213$) (Fig. 5E). No significant between-group differences were observed in emotional processing task performance or neuropsychological measures among men participants. In addition, there were no significant findings in women participants.

The rs2765 SNP decreases *TAC3R* mRNA expression in men

Human postmortem samples were used to determine *TAC3R* mRNA levels in rs2765 SNP carriers. Quantitative real-time polymerase chain reaction (qPCR) analysis of these samples revealed decreased expression of *TAC3R* mRNA in men carrying the rs2765 SNP in the *TAC3R* but not in women (sex by genotype $P = 0.049$; in men: AA

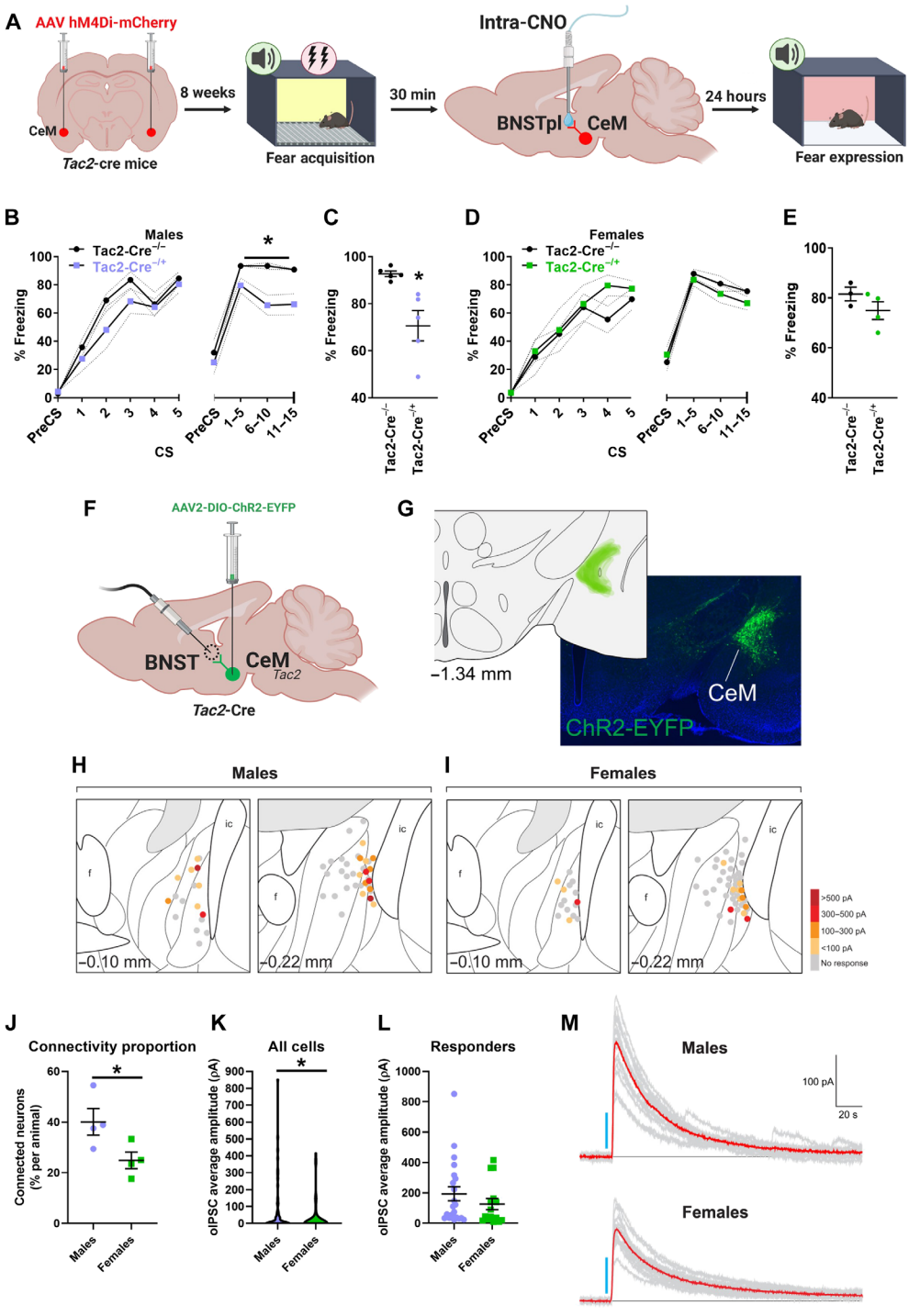

Fig. 3. Silencing *Tac2* neurons projecting from CeM to the lateral posterior BNST. (**A**) Experimental timeline. Created with BioRender.com. (**B** and **C**) Fear acquisition and FE in male mice receiving local-lateral posterior BNST (or STPL) CNO infusion after FA. (**D** and **E**) Fear acquisition and FE in female mice receiving local-lateral posterior BNST CNO infusion after FA. (**F**) Schematic representation of the slice electrophysiology experimental setup. Created with BioRender.com. (**G**) Representative image of viral infection and accurate targeting of the CeM in *Tac2*-Cre$^{-/+}$ mice. (**H** and **I**) Schematic of the anatomical location of representative traces of electrophysiological recordings in male (left) and female (right) mice. Dots represent the location of recorded neurons in the BNSTpl of *Tac2*-Cre$^{-/+}$ mice relative to major anatomical landmarks. Color code represents the range of amplitudes of optically evoked inhibitory postsynaptic currents (oIPSCs). Anatomical schematics based on Paxinos and Franklin's The Mouse Brain in Stereotaxic Coordinates, 2012. ic, internal capsule; f, fornix. (**J**) Percentage of connected neurons per animal (in males: 21 cells from four mice; in females: 15 cells from four mice). (**K**) Mean oIPSC amplitudes across all recorded cells (males: 54 cells; females: 63 cells) and (**L**) mean oIPSC amplitudes specifically in responders (in males: 21 cells; in females: 15 cells). (**M**) Representative traces of electrophysiological recordings of oIPSC in male (top) and female (bottom) mice. Data are shown as mean ± SEM and analyzed using repeated measures ANOVA or Mann-Whitney's *U*. **P* < 0.05.

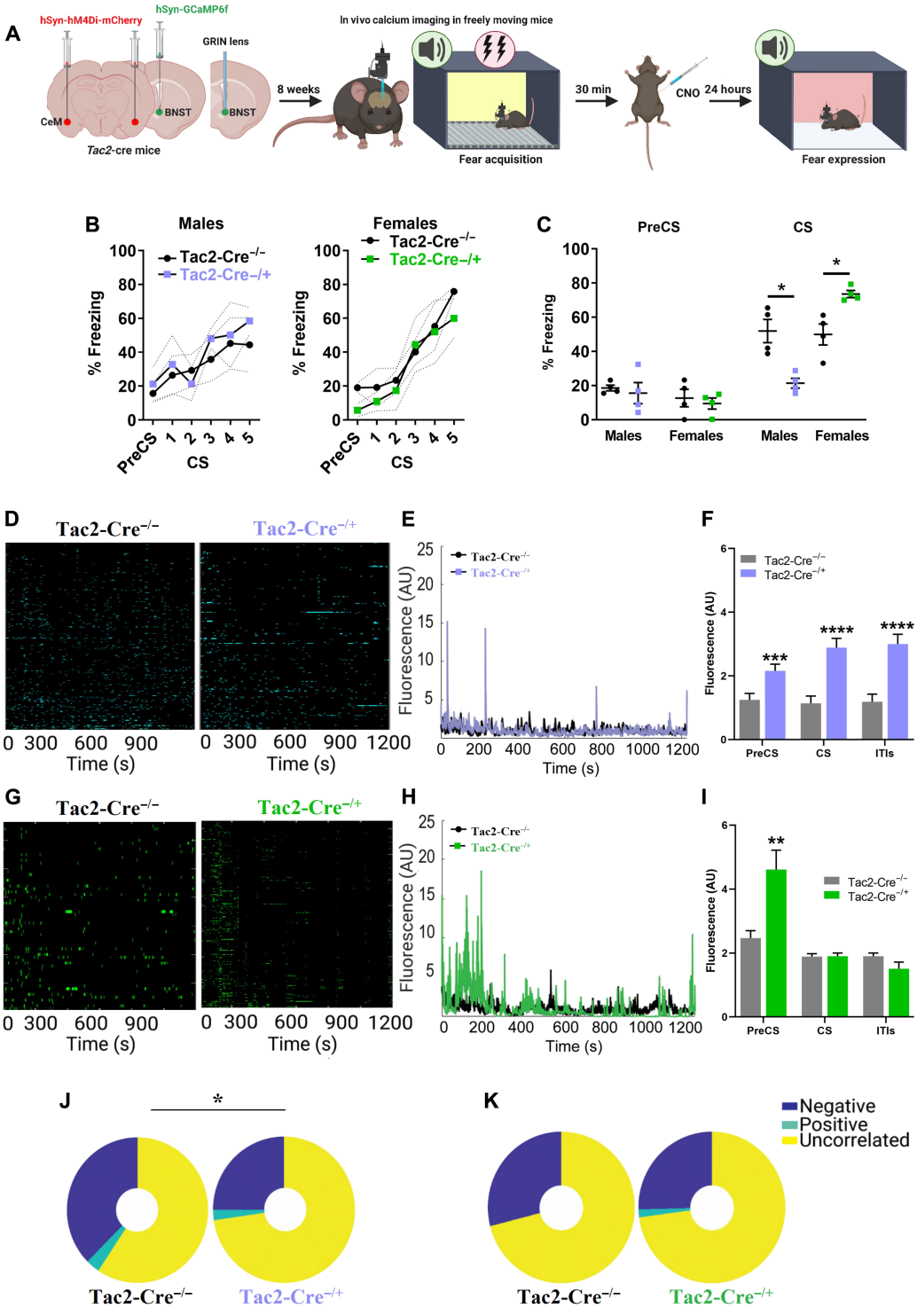

Fig. 4. Silencing *Tac2* neurons in the CeM reduces the proportion of significant correlations of calcium traces with freezing in males but does not affect this proportion in females. (**A**) Schematic timeline of the procedure. Created with BioRender.com. (**B**) *Tac2*-Cre$^{-/-}$ and *Tac2*-Cre$^{-/+}$ males and females show no differences during FA. (**C**) The average freezing during the preCS and all the CS was measured in FE. Temporarily silencing *Tac2* neurons in the CeM reduces memory consolidation in males and enhances it in females. (**D**) Heatmap representing the fluorescence of each neuron throughout the FE session in males. (**E**) Raw fluorescence in the lateral posterior BNST during the FE session in males. (**F**) Average raw fluorescence in males during the preCS, tone, and ITI. (**G**) Heatmap representing the fluorescence of each neuron throughout the FE session in females. (**H**) Raw fluorescence in the lateral posterior BNST (or STPL) during the FE session in females. (**I**) Average raw fluorescence in females during the preCS, tone, and ITI. (**J**) The proportion of neurons correlating with freezing in *Tac2*-Cre$^{-/-}$ and *Tac2*-Cre$^{-/+}$ males during the tone in FE. (**K**) The proportion of neurons correlating with freezing in *Tac2*-Cre$^{-/-}$ and *Tac2*-Cre$^{-/+}$ females during the tone in FE. Data are shown as mean ± SEM and analyzed using repeated measures ANOVA, Mann-Whitney's *U*, or Pearson's chi-square test. **P* < 0.05, ***P* < 0.01, ****P* < 0.001, and *****P* < 0.0001.

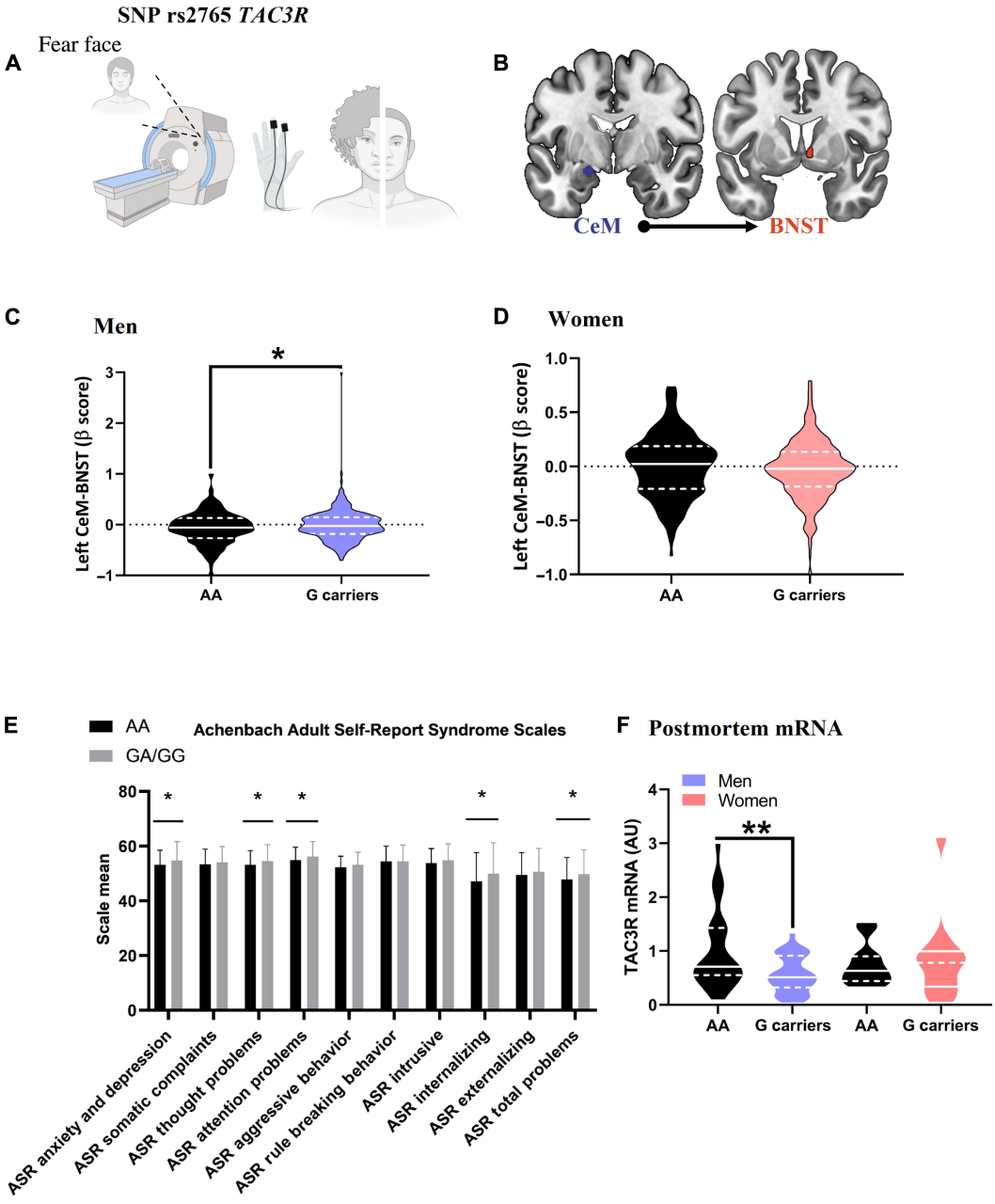

Fig. 5. The *TAC3R* SNP rs2765 decreases functional connectivity between the CeM and the lateral posterior BNST during threatening stimuli processing and reduces *TAC3R* mRNA expression in men but not in women. (**A**) Schematic representation of the experimental procedure. Created with BioRender.com. (**B**) Representative functional magnetic resonance imaging (fMRI) images illustrating the connectivity studied. (**C**) Left-CeM-BNST activation of the CeM and the BNST during the Hariri task in men. (**D**) Left-CeM-BNST activation of the CeM and the BNST during the Hariri task in women. (**E**) Achenbach Adult Self Report Syndrome Scales (ASR) for men. (**F**) Postmortem brain tissue analysis of *TAC3R* mRNA expression in men and women with and without the SNP. Data are presented as mean ± SEM except for (F), which is shown as mean ± SD; analyzed using one-way ANOVA, *t* test, Wald's chi-square, or Mann-Whitney's *U*. *$P < 0.05$ and **$P < 0.01$.

versus G carriers $P = 0.003$; in women $P = 0.723$) (Fig. 5F and tables S4 and S5).

The rs2765 and fear memory

Once the functional connectivity of CeM-*Tac2* neurons with the BNSTpl has been established in men and, to a lesser extent, in women, we proposed a subsequent experiment to investigate whether this pathway is involved in fear processing in humans in a sexually dimorphic manner (Fig. 6A). For this purpose, we hypothesize that the SNP rs2765 in the *TAC3R* alters the signaling of the pathway in men during fear processing, resulting in reduced fear memory, but this effect should be absent in women.

Genotype by sex frequencies and participants´ characteristics

Forty-nine of 130 participants (37.69%) were homozygous for the A allele in the rs2765 *TAC3R*, 62 (47.69%) had AG genotype, and 19 (14.61%) were homozygous for the G allele (allele frequencies: A

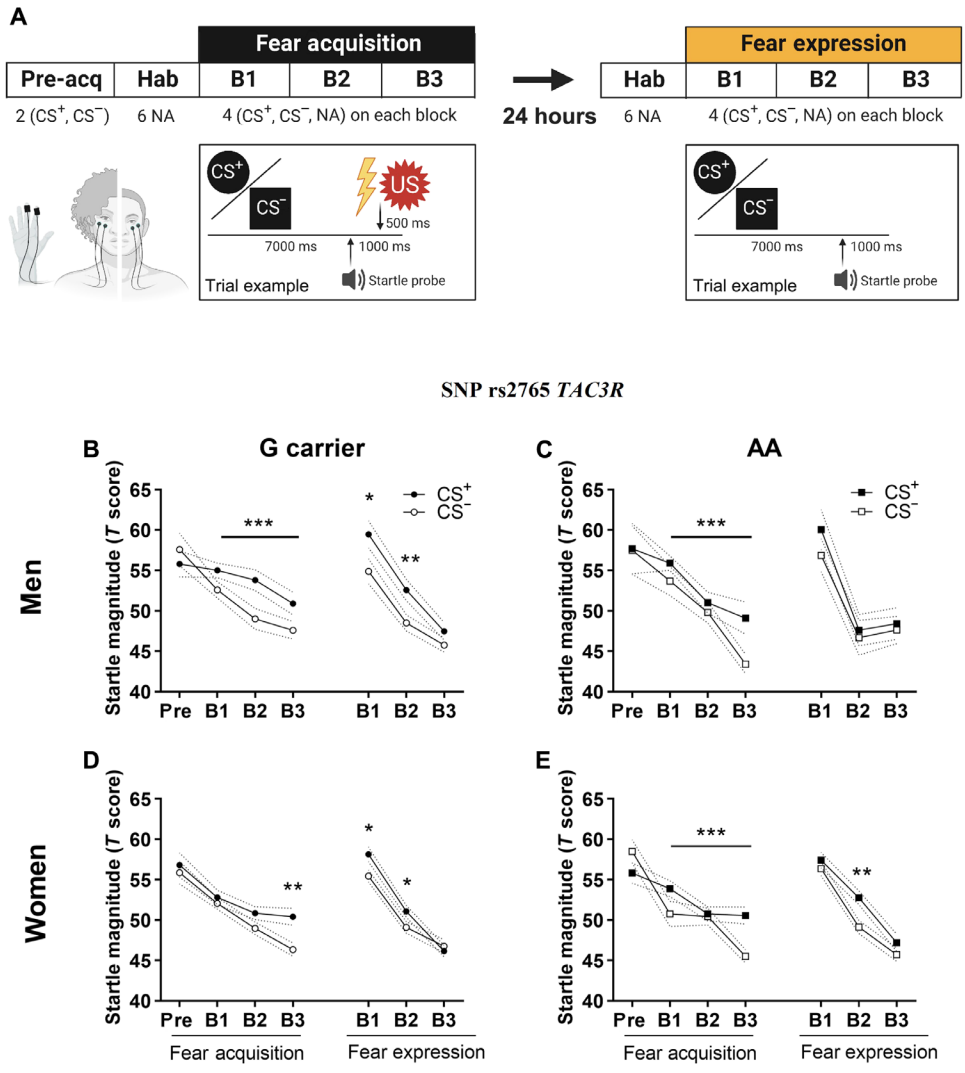

Fig. 6. Fear potentiated startle response with the *TAC3R* SNP rs2765 in men and women. (**A**) Schematic representation of the 2-day differential FA and FE task. B1, B2, and B3: block; CS^+: reinforced CS; CS^-: unreinforced CS; Hab: habituation phase; NA: noise alone; pre-acq: pre-acquisition phase; US: unconditioned stimulus. Created with BioRender.com. (**B**) G carrier men discriminated between the CS^+ and CS^- in the FA and FE. (**C**) AA carrier men discriminated between the CS+ and CS^- in the FA but not in the FE. (**D**) G carrier women and (**E**) AA carrier women discriminated between the CS+ and CS^- in the FA and FE. Asterisks above a line indicate significant main effect discrimination (CS^+ versus CS^- comparisons). Asterisks with no line indicate significant interaction between discrimination (CS+ versus CS^-) and specific blocks of trials. Data were analyzed using repeated measures ANOVA. *$P < 0.05$, **$P < 0.01$, and ***$P < 0.001$.

allele = 61.53%, G allele = 38.46%). Hardy-Weinberg equilibrium was verified for the present population ($P = 0.985$). Participants' characteristics by genotype group are presented in tables S6 and S7. Both groups had no significant differences in terms of age, sex, Spanish Version of the State-Trait Anxiety Inventory (STAI-T), unconditioned stimulus (US) intensity, US trials required for calibration, US discomfort, startle discomfort, and the proportion of contingency-aware participants.

The fear-potentiated startle

No significant main or interaction effects for stimulus, block, or genotype were found in the pre-acquisition phase. Evidence suggested a successful FA (i.e., higher response to the CS^+ than to the CS^-) as shown in a significant main effect of stimulus for the fear-potentiated startle (FPS) ($P = 0.001$) with significant CS^+ potentiation (CS^+ versus ITI, $P = 0.001$) and CS discrimination (CS^+ versus CS^-, $P = 0.001$). CS discrimination occurred since the first block (block 1, $P = 0.013$; block 2, $P = 0.031$; block 3, $P = 0.001$). Genotype had no significant main or interacting effects, and there were higher responses to the CS^+ than to the CS^- at the end of the FA ($P = 0.001$). Similar results were obtained using raw data (fig. S7).

During FE, there was a main effect for stimulus ($P = 0.001$) with significant CS^+ potentiation (CS^+ versus ITI, $P = 0.001$) and CS discrimination (CS^+ versus CS^-, $P = 0.001$). A stimulus by block interaction ($P = 0.001$) showed that CS potentiation (CS^+ versus ITI) was maintained throughout the whole FE session ($P = 0.001$), and CS discrimination disappeared in the last block of FE (block 1, $P = 0.008$; block 2, $P = 0.001$; block 3, $P = 0.301$) (fig. S7). We did not find a significant interaction stimulus by block by genotype ($P = 0.423$). However, the visual inspection of the graphs by genotype motivated within-group analyses. Both G carriers and AA subjects had significant

CS^+ potentiation ($P = 0.001$) and discrimination ($P = 0.001$). Further, a stimulus by block interaction in G carriers ($P = 0.001$) evidenced CS discrimination at block 1 ($P = 0.004$) and block 2 ($P = 0.001$) but not at block 3 ($P = 0.950$). In turn, AA subjects had impaired CS discrimination at early FE ($P = 0.001$; block 1, $P = 0.278$; block 2, $P = 0.014$; block 3, $P = 0.249$) (fig. S8).

Evidence from animal studies showed that the Tac2 pathway system has a sex-dependent regulation by sex during fear memory consolidation (*6*). Therefore, we analyzed separately the effects of genotype over FE on each sex.

In men, G carrier and AA participants showed a main effect of stimulus during FE with significant CS^+ potentiation ($P = 0.001$). G carrier men showed CS discrimination at block 1 ($P = 0.046$) and block 2 ($P = 0.005$) but not at block 3 ($P = 0.144$) (Fig. 6B). In turn, AA men had deficient CS discrimination ($P = 0.534$), and a trend-level stimulus by block interaction ($P = 0.066$) showed that this effect was because AA men had similar responses to the CS^+ and the CS^- throughout the whole FE (block 1, $P = 0.430$; block 2, $P = 0.806$; block 3, $P = 0.787$) (Fig. 6C). In women, both groups had significant CS^+ potentiation ($P = 0.001$). G carrier women presented evidence for CS discrimination since early FE ($P = 0.001$; block 1, $P = 0.034$; block 2, $P = 0.042$; block 3, $P = 0.544$) (Fig. 6D). However, in AA women there was no CS discrimination at early FE, although it was evident at later phases ($P = 0.001$; block 1, $P = 0.461$; block 2, $P = 0.004$; block 3, $P = 0.249$) (Fig. 6E). The analysis of the FPS in men suggests that the AA carrier phenotype is related to impaired fear memory consolidation compared to GG carriers, and this effect is not present in women.

The skin conductance response

The skin conductance response (SCR) showed no significant main or interaction effects for stimulus, block, or genotype during the preacquisition phase. There was evidence of successful FA (i.e., higher response to the CS^+ than to the CS^-) for SCR ($P = 0.001$) with significant CS discrimination (CS^+ versus CS^-; $P = 0.001$) (fig. S7). Genotype had no significant main or interacting effects, and we found higher SCR to the CS^+ than to the CS^- at the end of the FA ($P = 0.001$) (fig. S7). For FE, we found a significant main effect stimulus ($P = 0.001$) with significant CS discrimination ($P = 0.001$) (fig. S7). A trend-level stimulus by block by genotype interaction ($P = 0.083$) showed that AA subjects still had greater SCR responses to the CS^+ compared to the CS^- in the last block of FE ($P = 0.007$), as compared to G carriers ($P = 0.073$). A trend-level stimulus by block by genotype interaction ($P = 0.083$) showed that AA subjects still had greater SCR responses to the CS^+ compared to the CS^- in the last block of FE ($P = 0.007$), as compared to G carriers ($P = 0.073$). To test whether these differences were related to sex, separate analyses were carried out. Men showed a significant main effect stimulus ($P = 0.004$) with significant CS discrimination ($P = 0.004$). A trend-level interaction of stimulus by block by genotype ($P = 0.059$) showed that G carrier men had appropriate CS discrimination (greater responses to CS^+ than CS^-) at block 1 ($P = 0.001$) and that FE decreased ($CS^+ > CS$) throughout the session at block 2 ($P = 0.072$) and block 3 ($P = 0.443$) (fig. S9). In contrast, AA men did not discriminate between danger and safe cues neither at block 1 ($P = 0.236$) nor block 2 ($P = 0.876$) and showed higher responses to the CS^+ than to CS^- at the end of FE ($P = 0.027$) (fig. S9). This effect was also related to a significant decrease in SCR responses to the CS^+ between block 1 and block 3 in G carriers ($P = 0.001$) but not in AA men ($P = 0.253$) (fig. S9). In contrast, women presented a significant main effect stimulus ($P = 0.001$) with significant CS^+ discrimination ($P = 0.001$).

No genotype effects were found in women, and there were no relevant differences in subjective risk ratings in any genotype or sex (fig. S10). Together, these data support the involvement of the *TAC3R* SNP rs2765 in fear memory consolidation in men and not in women.

DISCUSSION

Our study reveals that the consolidation of identical fear memory processes undergoes sex-specific regulation in terms of neural projections within limbic forebrain circuits. These distinctions in the projections of *Tac2* neurons from CeM, in conjunction with other neuronal populations, play a crucial role in fear memory consolidation in both sexes. While *Tac2* neurons projecting to the BNSTpl demonstrate a necessary role in memory trace formation in males, the same projections in females appear to be dispensable for fear memory consolidation. This investigation highlights a high degree of similarity in the anatomical and functional architecture associated with the Tac2 pathway in CeM between mice and humans. In both species, the Tac2 pathway functional connectivity between CeM and BNSTpl is more pronounced in males. In addition, the disruption of normal functioning in this pathway is associated with negative valence emotionality in both species. Whether it is fear memory, perceived stress, or internalizing symptoms related to anxiety and depression, alterations in the Tac2 pathway are consistently linked to negative emotional experiences in mice and humans (Fig. 7).

The CeM-*Tac2* fiber silencing

Silencing *Tac2* fibers in the CeM significantly reduced fear memory consolidation in male mice, with no discernible effect observed in females during proestrus. Other reports have previously highlighted that proestrus is necessary for this manipulation to be effective (*6*). The reduction in the proportion of neurons correlated with freezing behavior following *Tac2* fiber silencing indicates a key role in the consolidation process. Notably, *Tac2* fiber silencing posttraining allows sufficient time for CNO clearance before the FE test (*6*). This experimental design isolated the drug's effect during the memory consolidation period. In males, *Tac2* fiber silencing led to reduced FE in the absence of the drug, signifying decreased consolidation compared to the control group. This reduction in FE correlates with increased calcium currents in the BNSTpl, aligning with previous studies demonstrating a supporting role of the BNST in the formation of fear memories (*16*, *17*). In addition, the proportion of neurons showing a statistically significant relationship, as measured by Pearson's *R* coefficient, with freezing behavior decreased in the *Tac2* silencing group compared to controls in males. Fluorescence of *Tac2*-$Cre^{-/+}$ males was higher in the preCS, CS, and ITIs compared to wild types, suggesting an overall increased neuronal activity in the BNSTpl during FE because of the temporal silencing of CeM-*Tac2* neurons after FA. Females' fluorescence did not increase in response to the tones, but *Tac2*-$Cre^{-/+}$ females exhibited increased fluorescence to the novel context before the first tone presentation. These data suggests that the temporal silencing of the *Tac2*-CeM to BNSTpl connectivity after FA modulates cued-fear memory and its neuronal activity during FE in the BNSTpl in males but not in females.

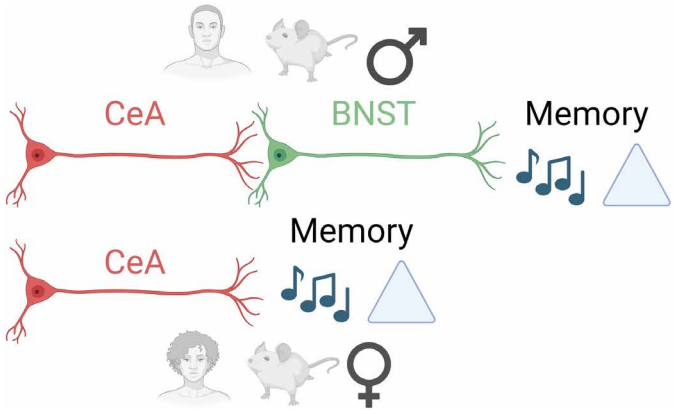

Fig. 7. Graphical abstract. We describe sex differences in neural projections for memory formation in both mice and humans.

Consistently, this gene has also been shown to be implicated in increased aggression associated with chronic social isolation in males (*18*, *19*). The effects of chronic social isolation have been shown to vary with various factors such as age, duration of isolation, or housing conditions, revealing sex differences, such as increased aggressive behavior in males and a greater increase in depressive-like and anxiety-like behaviors in females. The *Tac2* gene has been also demonstrated to be involved in the chronic stress-induced enhancement of aggression in male mice (*18*, *19*). Here, we demonstrate that the Tac2-mediated connectivity between the CeA and the BNST is stronger in males compared to females and that disruptions of this pathway may enhance vulnerability to psychopathology in humans.

Converging evidence of connectivity

Our design incorporates context-specific techniques for each field of research (*5*). In mice, viral tracing studies demonstrated increased expression of a reporter associated with adeno-associated virus (AAV) and Herpes simplex virus (HSV) in the BNSTpl of males compared to females after infecting *Tac2* neurons in the CeM. In humans, data from the HCP showed similar differences during a fear-processing task. Expanding on HCP data, we observed that a polymorphism in the *TAC3R* is associated with neurotic personality traits, internalizing symptoms of anxiety and depression, heightened perceived stress, and thought difficulties. These associations did not reach statistical significance in women, establishing the *TAC3R* polymorphism as a factor that renders vulnerability to psychopathology associated with internalizing symptoms in men but not in women.

mRNA levels and fear responses

Postmortem human tissue enabled us to assess mRNA levels in the brains of deceased individuals, both men and women. The findings reveal a decreased quantity of *TAC3R* mRNA in men carrying the AA allele compared to GG/GC carriers, a distinction not observed in women. Furthermore, using a well-established fear conditioning paradigm in human laboratory participants (*20*–*24*), we have linked this *TAC3R* polymorphism to lower startle response and diminished SCR. These two variables are widely recognized as indices of conditioned fear in humans. This evidence underscores the impact of the *TAC3R* polymorphism on molecular and behavioral aspects associated with fear conditioning, emphasizing sex-specific effects.

Potential implications and limitations of these results

This study suggests that the connectivity of CeM-*Tac2* neurons involved in fear memory processing is higher in males than in females in experiments involving mice and humans. In addition, we show that alterations in this Tac2 pathway (through chemogenetic silencing or the presence of an SNP) reduce fear processing in males but not females. However, other factors that have not been evaluated in this research and require further investigation may contribute to our found sex differences, including the presence of sex-specific fear coping strategies (*25*, *26*).

We acknowledge that one major limitation of this study is our current inability to precisely manipulate *Tac2* neurons in humans. The presented evidence suggests a potential therapeutic use of Tac2 antagonists (*27*–*29*). For instance, we hypothesize that dosing Tac2 antagonists shortly after trauma could decrease the likelihood of developing PTSD. An example of a Tac2 antagonist is Fezolinetant, recently US Food and Drug Administration–approved for treating hot flashes (*30*, *31*). We posit that exploring Fezolinetant in the context of conditioned fear and other psychopathological conditions with internalizing symptoms could offer valuable insights into the treatment of memory disorders. Notwithstanding, the potential impact of sex-specific effects reported suggests that while the Nk3R antagonist might be beneficial for males after traumatic stress, the enhancer effect in memory in females should also be considered and explored during extinction-based therapies. Last, our data may prove significant in areas of research involving behavior and neuronal projections, especially in contexts where sex differences have not been thoroughly explored or investigated.

MATERIALS AND METHODS

Ethics and biosecurity protocols

All experiments at the Autonomous University of Barcelona were performed under the ethics protocols approved for the experiments ref. CEEAH Ethics Committee on Animal and Human Research from the Universitat Autònoma de Barcelona (CEEAH) 3995, 6205, 6228, 6229, 6230, 6231, 6223, and 6235 and biosecurity protocols 345-16 and 407-17. All procedures were approved by the Committee of Ethics at the Universitat Autònoma de Barcelona and the Generalitat de Catalunya. They were also carried out following the European Communities Council Directive (2010-63-UE) and Spanish legislation (RD 53/2013). For the electrophysiology assay, experiments were performed following the ethical guidelines described in the National Institutes of Health (NIH) Guide for the Care and Use of Laboratory Animals and were approved by the Institutional Animal Care and Use Committee of the University of Connecticut Institutional Animal Care and Use Committee animal protocol number A22-056.

Animals

Male and naturally cycling female B6.129-*Tac2* < tm1.1(cre)Qima>/J [*Tac2*-Cre; B6;129S-*Tac2*tm1.1(cre)Hze/J; JAX stock #021878; RRID: IMSR_JAX:021878] were used, 8 weeks old at the beginning of the experiments. In some cases, *Tac2*-Cre mice were crossed to a Cre recombinase (Cre)–dependent tdT reporter line [B6;Cg-Rt(ROSA)26sor Tm14$^{(CAG-tdTomato)Hze}$/J or Ai14; JAX stock # 007914; RRID: IMSR_JAX:007914] (*32*, *33*), which selectively expresses tdT following Cre-dependent recombination. Animals were group-housed (two to four animals per cage) in a temperature-controlled

room (23° ± 1°C) throughout all experiments. Food and water were provided ad libitum.

Cued fear conditioning

In FA and FE tests, a computerized Startle system was used (Panlab-Harvard, Barcelona, Spain) (*6*, *34*). Delivery of tones and shocks was simultaneously controlled by Freezing v1.3.04 software (Panlab-Harvard, Barcelona, Spain). The fear chamber consisted of a black methacrylate box with a transparent front door (25 cm by 25 cm by 25 cm) inside a sound-attenuating chamber (67 cm by 53 cm by 55 cm). The same boxes were used for FA and FE.

Animals were habituated to the chambers for 5 min/day for two consecutive days before FA. For cue-dependent fear conditioning, all animals remained 5 min in the fear chamber before the onset of the first tone. During FA, all groups received five trials consisting of a tone as the CS (30 s, 6 kHz, 75 dB) that coterminated with a foot shock which served as the US (1 s, 0.3 mA). The ITI was 3 min, and 3 additional min followed the last trial. Pharmacological treatments were administered 30 min after FA to manipulate memory consolidation and avoid any effect during FA. The FE test was performed 24 hours after FA. For FE, mice remained 5 min in the chamber before trials and afterward were exposed to 15 trials of the 30 s CS tone alone (cued-fear) with a 0.5-min ITI interval. An additional 0.5-min interval followed the last trial of FE. Freezing behavior was used as an index of fear. Freezing behavior understood as a lack of any movement of the animal but for those related to breathing was recorded using the StartFear system, which allows recording and analysis of the signal generated by the animal movement through a high sensitivity weight transducer system.

To ensure that freezing behavior was exclusive of the previous tone-shock conditioning, different contexts were used for FA and FE. FA context consisted of a yellow light source (~10 lux), a grid floor of 25 bars (3 mm Ø and 10 mm between bars) that dispensed the foot shocks, the background noise of 60 dB produced by a ventilation fan, and a solution of ethanol (EtOH) 70% (v/v) odor was used for cleaning between sessions. FE context consisted of a red light source (~10 lux), a gray floor covering the bars, no background noise, and CR36—bronopol 0.26% (v/v), benzalkonium chloride 0.08% (v/v), and isopropyl alcohol 41% (v/v)—(José Collado, Barcelona, Spain) for cleaning, with changes in the length and turns of the transportation route from the vivarium to the testing room between FA and FE.

Vaginal smear cytology

Determination of the estrous stage in females was performed by assessing vaginal smear cytology. To assess the phase of the estrous cycle that female mice presented during FA, all female mice were monitored for 3 to 4 consecutive cycles (approximately 10 to 14 days) before learning to test for the regularity of the cycle. We performed a vaginal lavage with a 20-μl pipette that was loaded with 10 μl of standard NaCl 0.9% (w/v) solution, and later, the tip was softly placed on the vaginal aperture. In case of urination when grabbing the animal, urine was cleaned using a regular tissue. Male mice received the same amount of handling as female mice. The 10 μl of saline was unloaded and collected five consecutive times to collect enough cells for assessment and later placed on an adhesion slide (Superfrost Plus, Thermo Fisher Scientific, Barcelona, Spain). All vaginal smear samples were collected between 9:30 and 11:30 a.m. Slides were dried using a hot plate (HI1220, Leica, Madrid, Spain) at 37°C for 30 min and later stained in Cresyl Violet acetate (C5042, Sigma-Aldrich, Spain) 0.1% (v/v), washed twice for 1 min in distilled water, and read in bright-field microscopy with a 10× or 20× objective in an Eclipse 80i microscope (Zeiss, Spain).

Three different cell types may appear in the preparation: cornified epithelial cells, round nucleated epithelial cells, or leukocytes. The different stages of the estrous cycle were assessed depending on the proportion of the abovementioned cells. Proestrus is characterized by a high proportion (>80%) of nucleated epithelial cells that might present very small amounts of cornified epithelial cells or leukocytes. Estrus is typically presented with cornified epithelial cells with a lower grade of staining than leukocytes and nucleated epithelial cells. Metestrus presents a mixture of cornified epithelial cells and a considerable proportion of leukocytes. Diestrus is characterized by >90% of leukocytes that might present a very small proportion of round nucleated epithelial cells. After the assessment of regular cycling, females were distributed in groups according to the stage of the estrous cycle they presented before FA, which is also the day they received the CNO injection after FA (*6*).

For the electrophysiology experiment, vaginal swabs were collected for at least 1 week before sacrifice at proestrus, consistent with previous work (*6*, *35*). For identification of the estrous cycle stage, vaginal smears were stained using a Shorr stain (Sigma-Aldrich, catalog no. 109275). The staging was identified using the Track-by-Day method, predicting proestrus as 3 days after estrus. Estrus was identified by a fully cornified cell histology smear, appearing in sheets and clumps with little to no nucleated epithelial and leukocyte presence (*36*).

Surgeries

All surgeries were performed using isoflurane 5% (v/v) for induction and 2 to 3% (v/v) for maintenance, in oxygen, at a constant rate of 1.5 liters/min. After placing the mouse in the stereotaxic frame (Kopf Model 962, Harvard-Panlab, Barcelona, Spain) and after alignment of the antero-posterior (AP) and latero-medial (LM) axis with the frame, injections of 0.5 μl of AAV8-hSyn-DIO-hM4D(Gi)-mCherry, AAV2/1-Syn-WPRE-SV40-GCaMP6f, or H129ΔTK-TT in the CeM were performed or at a rate of 1 μl per 15 min to the CeM using the following coordinates: AP, −1.3; LM, ±2.5; and dorso-ventral (DV),–4.4 mm from Bregma. For cannulation, cannulae were placed bilaterally under the following coordinates: AP,–0.22; LM, ± 1; and DV, −3.25 mm from Bregma. Injections through the cannulae were performed with 1 mm of projection from the tip of the guide cannula at DV of −4.25 mm from Bregma. All references to brain regions are collected in table S1 for clarity.

Viral vector infection

We used two AAVs obtained from the plasmids pAAV-hSyn-DIO-hM4D(Gi)-mCherry [hM4di-mCherry Designer Receptors Exclusively Activated by Designer Drugs (DREADDs)] and pAAV-Syn-WPRE-SV40-GCaMP6f. The H129ΔTK-TT virus was donated by D. Anderson (*13*). AAV2-EF1a-DIO-hChR2(H134R)-EYFP was obtained from the University of North Carolina Vector Core, Deisseroth Lab. The AAVs AAV8-hSyn-DIO-hM4D(Gi)-mCherry and AAV2/1-Syn-WPRE-SV40-GCaMP6f were produced at the viral vector production unit at Universitat Autònoma de Barcelona. AAV8-hSyn-DIO-hM4D(Gi)-mCherry was bilaterally injected in the CeM (0.5 μl per side), and the AAV2/1-Syn-WPRE-SV40-GCaMP6f was unilaterally injected counterbalancing the injected hemisphere in the

BNSTpl, using a microinjection pump (coordinates and infusion rate abovementioned) (*6*).

Intraperitoneal injections, cannula placements, and micro infusions

Cannulae were placed using coordinates mentioned in the surgery section. For micro infusions of CNO in awake animals, internal cannulae projected 1 mm from the tip of the internal guide, reaching DV coordinate of −4.25 mm from Bregma during microinfusions, corresponding to the BNSTpl. Bilateral injections were performed simultaneously and manually using two knurled hubs, a type 3 tip, a 1-μl Hamilton syringe (external Ø 0.52 mm and internal Ø 0.26 mm) (Cibertec-Harvard, Madrid, Spain) coupled on one end to a polyethylene (PE) 50 tube (~20 cm) (Plastics One, Germany) with the internal cannula coupled to the other end of the tube. The PE-50 tube was filled with distilled water, leaving a 7.5-mm gap of air between the internal cannula and the water to avoid dilution of the drugs with water. Micro infusions were performed at a rate of 0.5 μl over 2 min, and internal cannulae remained one extra minute in place to prevent the backflow of the drug. CNO (Tocris) in 0.5% dimethyl sulfoxide (DMSO) (v/v) was dosed intraperitoneally at 1 mg/kg. The dose of CNO for intracerebral infusions was 1 mM in 0.5% DMSO (v/v).

Lens implantation

For the in vivo calcium imaging experiment, after receiving a bilateral injection of AAV8-hSyn-DIO-hM4D(Gi)-mCherry in the CeM, animals received a unilateral injection of AAV2/1-Syn-WPRE-SV40-GCaMP6f to the BNSTpl (coordinates mentioned above, 0.5 μl/7.5 min). Ten minutes after this injection, a knurl hub needle (26G) coupled to a 1-ml syringe was held with the syringe holder for stereotaxic devices, inserted over the BNSTpl at coordinates AP of −0.22, LM of ±1, and DV of −4.15 mm from Bregma, and left in place for 20 min while constantly lubricating the exposed surface with sodium chloride (0.9 g/liter). Once this needle is out, a straight Gradient-Index lens (Ø 0.6 mm, ~7.3 mm long, 0.5 Numerical Aperture, and pitch 3/2; catalog no. 1050-004597, Inscopix, USA). The last 0.1 mm until reaching the target is driven through the brain using the stereotaxic micromanipulator in a lapse of 10 min (Fig. 4A). The lens is secured with dental cement, and the lenses are covered with the plastic top of a 0.5-ml Eppendorf tube glued to the dental cement. The whole implant is covered with a fine layer of nontoxic silicon to ensure its protection.

Data analysis of calcium imaging

Microendoscopic videos of fluorescence in the BNSTpl were captured during the FE session in male and female *Tac2*-Cre$^{-/-}$ and *Tac2*-Cre$^{-/+}$ mice. Video motion was corrected using nonrigid motion correction, and calcium signals were extracted using Constrained Nonnegative Matrix Factorization (CNMF)-E. The raw traces of these signals were used to derive results.

For the analysis of the proportions of neurons correlated with behavior, we used second-to-second scores obtained with the software mentioned in the cued fear conditioning section. Raw fluorescence data were averaged for each second, and the Pearson correlation coefficient was established for the fluorescence of each neuron detected with CNMF-E (*37*) and the freezing score of the corresponding mouse. Neurons were then classified into three groups: negatively correlated ($R < -0.1$, $P < 0.05$), positively correlated ($R > 0.1$, $P < 0.05$), and not correlated or very low correlations ($-0.1 < R < 0.1$, $P < 0.05$ or any R value with $P > 0.05$).

In vitro slice electrophysiology

One- to 3-month-old male and female *Tac2*-Cre$^{-/+}$ and *Tac2*-Cre$^{-/+}$;tdT animals were bilaterally injected with 500 nl of AAV2-EF1a-DIO-hChR2(H134R)-EYFP in the CeM. Mice were group-housed and incubated with the virus for at least 10 weeks before slice electrophysiology experiments. For in vitro slice electrophysiology, male and female (proestrus) 4.5- to 6-month-old *Tac2*-Cre$^{-/+}$ or *Tac2*-Cre$^{-/+}$;tdT mice were anesthetized with isoflurane, followed by ketamine/xylazine injected intraperitoneally as previously described (*14*). Mice were transcardially perfused with 10 to 20 ml of ice-cold sucrose solution: 87 mM NaCl, 75 mM sucrose, 25 mM glucose, 25 mM $NaHCO_3$, 7.5 mM $MgCl_2$, 2.5 mM KCl, 1.25 mM NaH_2PO_4, 0.5 mM $CaCl_2$ and 5 mM ascorbic acid, bubbled with 95%O_2/5%CO_2. After decapitation, the brain was removed and immersed in an ice-cold sucrose solution. Coronal BNST sections at a thickness of 225 μm were obtained using a vibrating microtome (7000smz-2, Lafayette Instrument Company). Slices were incubated for 30 to 45 min at 34°C in artificial cerebrospinal fluid (ACSF): 125 mM NaCl, 25 mM $NaHCO_3$, 15 mM glucose, 2.5 mM KCl, 1.25 mM NaH_2PO_4, 1 mM $MgCl_2$, and 2 mM $CaCl_2$. After recovery, slices were then transferred to room temperature for at least 30 min before recording. Slices were placed in a recording chamber and continuously superfused with oxygenated ACSF (95%O_2/5%CO_2), and patch-clamp recordings were performed at room temperature using an upright Olympus microscope (Olympus America Inc.), Multiclamp 700B amplifier, and pClamp10 acquisition software (Molecular Devices). BNST slices that best corresponded to mouse brain atlas images (*38*), approximately −0.10 to −0.30 mm from Bregma, were used to identify neurons in the posterior BNST between the fornix and internal capsule. Whole-cell voltage-clamp recordings were performed from BNST neurons using the following low chloride, cesium-based internal solution: 135 mM $CsMeSO_3$, 10 mM Hepes, 1 mM EGTA, 1 mM $MgCl_2$, 3.2 mM tetraethylammonium chloride, 0.1 mM spermine, 5 mM Na_2-phosphocreatine, 4 mM Mg–adenosine triphosphate, and 0.3 mM Na–guanosine triphosphate (288 mOsm/liter, pH 7.3). Borosilicate pipettes (resistances of 2.5 to 5 megohm) were used to obtain tight seals of >1 gigaohm before rupturing the membrane. Only recordings with a stable series resistance of <20 megohm were included in the data analysis. Cells were held at 0 and −70 mV, and ChR2-EYFP–expressing CeM fibers were photostimulated (single 5-ms pulses) through whole-field illumination with blue light (~470 nm) using a transistor-transistor logic (TTL)–controlled white light-emitting diode (Sutter Instrument Company), transmitted through a green fluorescent protein filter cube (Olympus America Inc.) and a 60× objective (Olympus America Inc.) at a frequency of once per 20 s. oIPSCs were detected in a subset of neurons. All data were analyzed with ClampFit (Molecular Devices).

Immunohistochemistry

For immunohistochemistry assays, mice were transcardially perfused with 50 ml of 4% (v/v) paraformaldehyde (PFA) (Casa Álvarez, Spain) for 5 to 6 min and then decapitated, and brains were extracted and stored in 4% (v/v) PFA for 24 hours. After this time, brains were rinsed (three times, 10 min each) with 1× Sorenson's PB consisting of sodium phosphate dibasic (10.9 g/liter; Sigma-Aldrich, Spain) and sodium phosphate monobasic (3.2 g/liter; Sigma-Aldrich, Spain) and

transferred into 30% sucrose (Sigma-Aldrich, Spain) in 1× Sorenson's PB in conic Falcon tubes (Thermo Fisher Scientific, Spain) until the brain reached the bottom of the tube (~48 to 72 hours). Right after, brains were snap-frozen in a metal cube containing isopentane (Sigma-Aldrich, Spain) cooled with dry ice and stored at −80°C until sectioning.

For cFos fluorescent immunostaining, brain sections (30 μm per section) were rinsed three consecutive times with 1× KPBS. All incubations were performed on top of a shaking platform. Right after washing the slices, these were incubated for 60 min in blocking buffer (5% donkey serum and 0.4% Triton X-100 in 1× KPBS) at 4°C. After incubation in blocking buffer, sections were incubated overnight with the mouse monoclonal antibody to cFos (ab20894, Abcam, The Netherlands). The primary antibody was diluted in 0.4% Triton X-100 in 1× KPBS. After incubation in the primary antibody solution, brain slices were rinsed three times with KPBS 1× and then incubated in a secondary antibody solution for 2 hours at room temperature. The secondary antibody solution was prepared in Triton X-100 (×100, Sigma-Aldrich, Spain) 0.4% (v/v) in 1× KPBS and included secondary antibody donkey anti-mouse Alexa Fluor 647 conjugated to fluorophores (1:1000; 715-606-150, Jackson ImmunoResearch), and 4′,6-diamidino-2-phenylindole (DAPI) (1:10,000; 10236276001, Sigma-Aldrich) was used to stain cell nuclei. Z-stacks of the CeA (0.50 μm per interval) were acquired using a Leica SP5 confocal microscope (Leica, Spain) with a PL 20×/1.25 to 0.75 objective controlled by LAS X v2.7.3.9729 software (Leica, Spain). cFos-positive neurons were determined using the cell count plugin from Fiji for Windows v1.52. n. The integrated density of the mCherry and tdT signals was interpreted as a measure of protein expression. The average cFos count and mCherry integrated density between the right and left hemispheres' signals were calculated for four to six pictures and averaged for each animal for statistical analyses.

Cannula, lens, and injection placement verifications

For cannula and lens placement verifications, amygdala and BNST brain sections were stained with a standard Nissl staining protocol, respectively. Brains were sectioned (30 μm per section) using a Leica cryostat (−21°C for the chamber, −19°C for the sample), direct to mount, and stored at −20°C until staining. Slides were dried on a hot plate at 37°C overnight before staining. First, slides were dehydrated in consecutive decreasing concentrations of denaturalized EtOH (Casa Álvarez, Spain): 3 min in EtOH 100% (v/v), 3 min in EtOH 95% (v/v), and 3 min in 70% (v/v). Right after that, slides were rinsed in distilled water three times for 2 min each to extract any trace of sucrose. Samples were then stained for 8 min in a Cresyl Violet Acetate Solution consisting of Cresyl Violet Acetate (1 mg/ml) in a Walpole Solution, prepared with glacial acetic acid (Sigma-Aldrich, Spain) 60% (v/v) and 0.2 M sodium acetate (Sigma-Aldrich, Spain) 40% (v/v). After staining, slides are rinsed twice in distilled water for 2 min each and then dehydrated using increasing concentrations of EtOH: 3 dips in EtOH 50% (v/v), 3 dips in EtOH 70% (v/v), 3 dips in EtOH 96% (v/v), and 3 min in EtOH 100% (v/v). After this last dehydration, slides are incubated in xylene (Sigma-Aldrich, Spain) three times for 3 min each and then covered using DPX mountant for histology (Sigma-Aldrich, Spain). Slides remain untouched for 24 hours in the dark until stored in a regular box for slides at room temperature. Cannulae and lens placement verification was performed using bright-field photographs obtained using a 10× objective in an Eclipse 80i microscope (Leica, Spain). Animals that did not present a bilateral cannula lesion in the CeA were discarded from experiments.

Further, one or two slices from the BNST were mounted, stained with DAPI, and covered using fluoromount (Sigma-Aldrich, Spain) to ensure that the injection site matches the lens place. To confirm the localization of the bilateral injection sites in the CeM for electrophysiology assays, the unsliced portion of the brain was drop-fixed in 4% PFA overnight at 4°C following slicing for electrophysiology. For cryoprotection, the tissue was transferred to 30% sucrose for 24 to 48 hours and flash-frozen using isopentane on dry ice. Sections containing the CeM (40-μm thick) were taken on a cryostat (Leica CM3050S) and mounted using VECTASHIELD Hardset Antifade mounting medium (Vector Laboratories, catalog no. H1400). Fluorescent 10× microphotographs of the CeM injection site were visualized on a Keyence BZ-X700 and confirmed before the analysis of electrophysiology data.

Human connectome project

HCP is a consortium effort for the mapping of brain function that provides multimodal neuroimaging and behavioral data for biomedical research, including comprehensive genotyping of SNPs available through the database of Genotypes and Phenotypes (ethics ID #2022-23170-25554-3 from the University of Melbourne).

Participants

From an initial pool of 1206 healthy young adults, 1044 had completed an emotional matching functional magnetic resonance imaging (fMRI) paradigm, and 984 of those had available information regarding the rs2765 SNP of the NK3-R–coding gene TACR3 (age range = 22 to 36 years; age mean = 28.75; SD = ±3.69; 53% women). Self-reported racial identity was predominantly white (76.4%; 11% Hispanic/Latino), followed by Black/African American (13.7%) and Asian/Hawaiian (5.9%). Regarding socioeconomic status, the household income of our participants was centered around the US national average (*39*). The genomic distribution of the rs2765 SNP followed the expected pattern (*40*), with only 14.3% of the sample expressing alleles GG.

Neuroimaging analyses

To evaluate the functional connectivity between the superficial–centromedial amygdala (sf/cmA) and the BNST during the processing of aversive stimuli, we selected task-based fMRI data derived from an adaptation of a well-validated emotion processing paradigm (*41*, *42*). Briefly, the participants were asked to signal via a controller which of the two stimuli (left/right) matched a third stimulus presented at the top of the screen, alternating between blocks of trials with either angry/fearful facial expressions or neutral shapes. Measures of accuracy (percent correct match) and mean reaction time (milliseconds) were collected.

Preprocessed fMRI images were obtained [see (*43*) for a detailed explanation of the specific preprocessing steps] from the S1200 open-access release of the HCP Young Adult study (*42*–*44*). Using Statistical Parametric Mapping 12 (SPM12) software (*44*), preprocessed fMRI images were additionally smoothed with an 8-mm full width at half-maximum isotropic Gaussian kernel to increase the signal-to-noise ratio. First-level contrast images were calculated for each participant. Specifically, emotional reactivity was assessed by contrasting fearful face trials to neutral stimulus trials. Motion parameters previously estimated from a rigid-body transformation to the first image acquired (original and temporal derivatives) were also added as regressors to correct movement during the scanning. In addition, the Blood

Oxygenation Level Dependent signal was convolved with the SPM12 canonical hemodynamic response function, and a 128-s high-pass filter was used to remove low-frequency drifts.

First-level contrast images for each participant were then included in a psychophysiological interaction analysis to explore the impact of emotional reactivity (fearful faces > neutral stimulus) on the strength of time-course correlations between the sf/cmA and the BNST. From each individual contrast image, we extracted the signal from two seed regions of interest (one per hemisphere), located at the sf/cmA nucleus of the amygdala. Seeds were defined with the MarsBar region-of-interest toolbox (*45*) as 3.5-mm radial spheres centered at the following Montreal Neurological Institute coordinates [following Baur *et al.* (*46*) proposal]: left sf/cmA ($x = -19$, $y = -5$, $z = -15$) and right sf/cmA ($x = 23$, $y = -5$, $z = -13$). For the BNST, we used a bilateral mask defined in Torrisi *et al.* (*47*). Task-based functional connectivity maps were estimated for each seed using linear regression analyses. The resulting images were then included in two-sample t test models (one per sex) to assess between-group effects (AA versus GA/GG). Voxels surviving a family-wise error (FWE) small-volume corrected significance threshold of $P < 0.05$ were deemed significant.

Psychological evaluation

Participants completed a vast array of neuropsychological tests assessing episodic memory [NIH Toolbox Picture Sequence Memory Test (*48*) and Penn Word Memory Test (*49*)], executive function [Dimensional Change Card Sort (*50*) and the flanker task (*51*)], fluid intelligence [Penn Progressive Matrices (*52*)], language [Oral Reading Recognition Test (*53*) and Picture Vocabulary Test (*54*)], processing speed [Pattern Comparison Processing Speed Test (*55*)], spatial orientation [Variable Short Penn Line Orientation Test (*56*)], sustained attention [Short Penn Continuous Performance Test (*49*)], and emotion recognition [Penn Emotion Recognition Test (*49*)].

Psychopathology evaluating scales were also administered: the Achenbach Adult Self-Report Syndrome Scales (*57*, *58*), the Achenbach DSM-Oriented Scale (*58*), and the Semi-Structured Assessment for the Genetics of Alcoholism scale (*59*). Other mental health dimensions were assessed, including personality traits [NEO-FFI (*60*)], perceived negative affect, psychological well-being, stress, and self-efficacy. In addition, data about anxiety and depression history in participants' parents were also acquired.

Human behavior analyses

We assessed in-scanner task performance data regarding accuracy (percent of correct matching of stimuli) and reaction times (milliseconds) during both conditions of the emotional processing task (faces and shapes), as well as measures of the differential task performance (faces-shapes).

Postmortem tissue analysis

Subjects and samples

Human brain samples were obtained from autopsies performed at the Basque Institute of Legal Medicine (IVML, Bilbao, Spain). The study was carried out following Spanish ethical standards for postmortem brain studies and with the Declaration of Helsinki.

Samples of the dorsolateral prefrontal cortex (Brodmann's area, 9) from a total number of 173 subjects (134 men and 39 women) were collected, dissected, and immediately frozen and stored at −70°C. The mechanism of death was accidental for all of them as determined by medical examination, being a traffic accident for $n = 132$. Retrospective information about possible diagnosis and treatment was obtained from the medical examiner's information and antemortem medical records so that evidence of neuropsychiatric disorder could be ruled out for all the subjects. Toxicological screening for the detection of psychotropic drugs and EtOH on blood was performed at the National Institute of Toxicology, Madrid, Spain. To cope with the haplotype diversity between different ethnic groups, this study was performed in a homogeneous set of Caucasian subjects of European origin. The demographic characteristics, mechanism of death, and toxicology in the blood are shown in table S4. These subjects had been previously included in other studies (*61*).

SNP rs2765 genotyping

Genomic DNA (gDNA) was extracted from brain tissue under blind conditions using standard procedures (*62*). Genotyping was carried out using TaqMan assay (C___1340532_10; Applied Biosystems, Foster City, CA, USA). Reactions were carried out in a 5-μl total reaction volume containing 22.5 ng of gDNA. Allelic discrimination plots for genotyping data were analyzed by StepOne Software v2.1 (Applied Biosystems).

mRNA expression and cDNA synthesis

Of the 173 genotyped subjects, total RNA was extracted from 124 samples using a commercial RiboPure kit (Thermo Fisher Scientific, Waltham, MA, USA) according to the manufacturer's instructions. RNA concentration and quality were measured in a NanoDrop 1000 Spectrophotometer (Thermo Fisher Scientific). RNA integrity number (RIN) was also assessed for RNA quality in the Agilent 2100 Bioanalyzer (Agilent, Santa Clara, CA, USA) using an Agilent RNA 6000 Nano kit and RNA Nano chips following the manufacturer's instructions (see table S4 for obtained RIN values). One microgram of total RNA was converted to single-stranded cDNA using a High-Capacity cDNA Reverse Transcription kit (Thermo Fisher Scientific) following the manufacturer's instructions.

Quantitative real-time polymerase chain reaction

mRNA expression of *TACR3*, *GAPDH*, and *RPS13* reference genes was assessed by qPCR using predesigned TaqMan assays (see table S5). The final volume for each reaction was 10 μl with 40 ng of cDNA in the case of TACR3 and 5 μl with 20 ng of cDNA in the case of reference genes. All samples were run in triplicates. Each run included a negative water control.

Fear-potentiated startle

Participants

The study was approved by the Ethics Committee on Animal and Human Research from the Universitat Autònoma de Barcelona #3995 and conducted in accordance with the Declaration of Helsinki (2008). Potential participants (healthy adults, age ≥ 18, $n = 620$) were invited to participate through advertisements or email in a study "on emotional memories." In an intake session, they were informed about the study, and inclusion and exclusion criteria were assessed by a physician using an ad-hoc semistructured clinical interview. Inclusion criteria were age > 18 and not having taken any psychotropic drug during at least 1 month before the study. Exclusion criteria were age over 45, current drug abuse, mental, neurologic, or endocrinologic disorders, and current use of medications acting on the endocrine or central nervous system. Those fulfilling inclusion criteria and accepted to participate ($n = 145$) signed informed consents, completed the STAI-T (*63*), provided a 2-ml saliva sample, and were scheduled for the first experimental session. Participants were asked to abstain from alcohol for 24 hours, caffeine for 12 hours, and food for 2 hours before each experimental session. Thirteen participants

declined to participate in the day 2 session, and two participants were excluded due to technical problems. The final sample consisted of 130 participants (97 women, 33 men; age = 23.4, SD = 4.6). Participants completing the study received €20 as compensation.

Study overview

All participants underwent a 2-day experimental protocol where SCR, FPS, and subjective risk ratings were assessed during FA (day 1) and FE (day 2, 24 hours after). Saliva samples were collected in both sessions.

Stimuli and procedure

The conditioned stimuli (CSs) were two geometric figures (a square and a circle) presented on a computer screen for 8000 ms. The US was an electric shock of 100 ms delivered to the nondominant forearm. The US was generated by a stimulator (Grass Instruments S48, USA), isolated (SIU5), and transmitted via a constant current unit 1 to a bipolar bar electrode (EP10-621, Technomed Europe, The Netherlands). The startle probe was a 50-ms burst of white noise at 102 dB, with near-instantaneous rise time, delivered binaurally through high-fidelity headphones. Online ratings of US expectancies (risk ratings) for each CS were obtained using a scale presented on the screen (0 = no risk, 9 = high risk) after each CS presentation. Stimulus presentation and timing were controlled with the software Affect 4.0 (KU Leuven, Belgium) (*64*).

On day 1, participants gave a 2-ml saliva sample and completed the STAI-S (*63*). After this, the recording and shock electrodes were attached, the intensity of the US was adjusted (to an intensity that was "highly uncomfortable but not painful"), and the headphones for the startle probes were placed. Participants were told that they could receive an electric shock during the experiment and that they would be able to predict its occurrence if they paid close attention to the presentation of the figures. They were also explicitly told to ignore the acoustic startle probes and were asked to assess the risk of shock for each CS presentation using a 0 to 9 scale (from "no risk of shock" to "maximum risk of shock"). During the fear pre-acquisition, two nonreinforced presentations of each CS occurred, followed by a habituation phase with six presentations of the startle probe alone. During FA, one of the CS was paired to the US 500 ms before CS the offset (CS^+) at an 83% reinforcement rate, while the other CS was not (CS^-). A fixation cross appeared during the ITIs. Trial order was pseudorandomized and counterbalanced across CS, with no more than two presentations of a specific CS occurring in a row. Startle probes appeared 1000 ms before the end of the CS presentation, in 66% of the FA trials. ITIs and interprobe intervals ranged from 10 to 14 s and 18 to 22 s, respectively. The FA phase consisted of 12 presentations of each of the CS^+, CS^-, and noise alone (NA). All participants received 12 CS^+, 12 CS^-, and 47 participants received 10 NA and the other participants 12 NA. The selection of the figure used as CS^+ was counterbalanced between subjects. After the task, participants completed again the STAI-S, rated the discomfort associated with the startle probe and the US (0 = no discomfort, 9 = maximum discomfort), and answered a question to assess contingency awareness ["The electric stimulus appeared along with a) the circle, b) the square, c) there was no association, d) I don't know"].

On day 2, participants followed the same recording and calibration procedures as for day 1, but they were instructed that they may better predict the appearance of the electric shock if they recall what they experienced in the previous session. This was followed by a habituation phase with six presentations of the startle probe alone and the FE phase, with 12 presentations of each of the CS^+, CS^-, and NA. All participants received 12 CS^+, 12 CS^-, and 47 participants received 10 NA and the other participants 12 NA. No USs were administered during day 2.

Physiological recordings and response definition

Physiological data were recorded using a BIOPAC MP 150 (BIOPAC Systems Inc., USA) and AcqKnowledge 4.1.0 software. SCR were recorded by attaching two Ag-AgCl electrodes filled with hydrogel to the middle and index fingers of the nondominant hand. The signal was sampled at 125 Hz, and SCR magnitudes were computed as the difference between the maximum SCR and the value at response onset, detected in 1 to 6 s after stimulus onset. Only trials with deflections starting between 1 and 4 s after stimulus onset were considered valid. When two clearly separated peaks in the SCR were visible, only the maximum SCR response of the first peak was considered. Trials with no response, or magnitudes < 0.01 μS, were considered no-response trials and scored as 0. Trials with excessive baseline or artifacts were discarded (0.25% for FA and 0.77% for FE).

Startle blink responses were measured by recording the electromyographic (EMG) activity of the orbicularis oculi using two 0.5-cm Ag-AgCl surface electrodes. The raw EMG signal was sampled at 2 kHz and filtered (analog 50-Hz notch filter; and digital infinite impulse response band-pass filter, cut-off frequencies of 28 and 500 Hz), rectified, and smoothed (20-ms moving window average). FPS responses were considered valid if the elevation in the EMG observed after the startle probe started between 20 and 100 ms, with its peak occurring between 20 and 150 ms (*65*). Startle amplitudes were computed by subtracting the mean response in microvolts of the 50 ms preceding the startle probe from the response peak value. Trials where no response was detected were scored as 0. Trials with excessive baseline or artifacts were discarded (2.37% for FA and 1.65% for FE).

After visual inspection (performed blind to genotype), participants showing nonvalid SCR responses in 70% of US trials during FA were classified as physiological nonresponders ($n = 1$), and all SCR trials for these participants were scored as missing values and discarded. Similarly, individuals showing nonvalid responses in 70% of habituation startle probes were classified as physiological nonresponders ($n = 2$ FA, $n = 0$ FE). Nonresponders were identified using raw SCR and raw FPS data (*66*, *67*).

SNP rs2765 genotyping

Saliva was collected into polypropylene tubes using the passive drool method and frozen at −80°C until analysis. gDNA was extracted using the ATP TM Genomic DNA Mini Kit Tissue (ATP Biotech Inc., Taiwan). DNA was quantified and diluted with deoxyribonuclease-free water to 5 ng/μl. The rs2765 *TAC3R* was determined using the TaqMan Genotyping Master Mix (Applied Biosystems, USA) and the TaqMan SNP Genotyping Assay, human #4351379 assay C___1340532_10 (Thermo Fisher Scientific, Spain). The final volume for qPCR reaction contained 10 ng of gDNA. Cycling parameters included 10 min at 95°C, followed by 40 cycles of denaturation for 15 s at 95°C and 1 min at 60°C for annealing/extension. PCR plates were read in an ABI 7500 fast system instrument with 7500 Software v2.3 (Applied Biosystems, USA).

Data analyses

Statistical analyses were performed using IBM SPSS Statistics 23.0, MATLAB 2023b (MathWorks, 2023) or R (R Core Team R Foundation for Statistical Computing, 2021). Detection of outliers was done using Grubbs test and removed when it was appropriate

(*68*). Sample sizes were determined on the basis of previous literature. When possible, subjects were pseudorandomly assigned to the different experimental groups, and data were codified during collection and decodified for analyses. For experiments involving independent samples, when these presented normal distributions and equality of variances (Shapiro-Wilk's and Levene's test, respectively), one-way ANOVA or *t* test from the general linear model was used; otherwise, nonparametric analyses were used for one-factor analyses. Wald's chi-square with pairwise comparisons was used in the generalized linear model for multifactorial analyses that did not accomplish normality or homoscedasticity. For related sample analyses, two-way repeated measures ANOVA was used to assess sex-by-genotype/treatment interactions. For repeated measures ANOVA, we used trials for FA or mean of groups of five trials for the FE test as a within-subject variable. Equality of variances and sphericity were tested. When sphericity could not be assumed, Greenhouse-Geisser statistics were used for assessing the significance, and the corrected degrees of freedom were provided. ANOVA was used for the evaluation of simple main effects and when an interaction between main effects was significant. Pearson's *R* coefficient was used to assess significant correlations, and cFos cell count in each expressing area was used to calculate the correlation matrices and fold change for each group.

For postmortem tissue analysis, mRNA expression of target gene *TACR3* was corrected with that of reference genes *GAPDH* and *RPS13* and with a reference sample (pool of control samples) using ΔΔCt method: ΔΔCt = [Ct (target gene) sample − Ct (reference gene) sample]–[Ct (target gene) reference sample − Ct (reference gene) reference sample]. The relative amount of mRNA was calculated as $2^{-\Delta\Delta Ct}$. For FPS experiments, we assessed in-scanner task performance data regarding accuracy (percent of correct matching of stimuli) and reaction times (milliseconds) during both conditions of the emotional processing task (faces and shapes), as well as measures of the differential task performance (faces-shapes). In addition, we also evaluated the neuropsychological and mental health measures available in the HCP dataset (see table S3). Data were analyzed by performing two-sample *t* tests to compare task performance as well as neuropsychological and mental health scores between rs2765 SNPs in women and men. A significance threshold of $P < 0.05$ was adjusted using a false discovery rate to account for independent comparisons.

Data availability

The research team has signed an agreement with the HCP to obtain access to restricted data to carry out the presented research. We used both tier 1 (nonsensitive but potentially identifying) and tier 2 (sensitive and potentially identifying) data in our analysis. In accordance with the terms of this agreement, we cannot share the provided access with individuals or organizations that have not already been granted access by HCP. Postmortem brain samples used in this study belong to a private brain collection managed by its legal responsible J. J. M. Martínez. This brain collection is registered in the Official Registry of the Spanish Health Institute Carlos III (number 35). Processes related to sample obtention and utilization comply with the Spanish Law 14/2007, RD 1716/2011 (BOE 2 December) and the collaboration agreements between the University of the Basque Country and the original institutions. The brain samples were used in the context of a collaboration between members of the neuropsychopharmacology group in the UPV/EHU, led by J. J. M. Martínez and of whom G. Rivero is part. The material transfer agreement which specifies the boundaries for the utilization of these samples was submitted to Science Advances. All the other datasets obtained and analyzed in the study are in https://doi.org/10.34810/data1172.

Supplementary Materials

This PDF file includes:

Figs. S1 to S10
Tables S1 to S7
Legend for data S1
Legend for movie S1

Other Supplementary Material for this manuscript includes the following:

Data S1
Movie S1

REFERENCES AND NOTES

1. E. R. Kandel, The molecular biology of memory storage: A dialogue between genes and synapses. *Science* **294**, 1030–1038 (2001).
2. E. R. Kandel, Y. Dudai, M. R. Mayford, The molecular and systems biology of memory. *Cell* **157**, 163–186 (2014).
3. E. R. Velasco, A. Florido, M. R. Milad, R. Andero, Sex differences in fear extinction. *Neurosci. Biobehav. Rev.* **103**, 81–108 (2019).
4. J. P. Johansen, C. K. Cain, L. E. Ostroff, J. E. Ledoux, Molecular mechanisms of fear learning and memory. *Cell* **147**, 509–524 (2011).
5. Á. Flores, M. À. Fullana, C. Soriano-Mas, R. Andero, Lost in translation: How to upgrade fear memory research. *Mol. Psychiatry* **23**, 2122–2132 (2018).
6. A. Florido, E. R. Velasco, C. M. Soto-Faguás, Á. Gomez-Gomez, L. Perez-Caballero, P. Molina, R. Nadal, Ó. J. Pozo, C. A. Saura, R. Andero, Sex differences in fear memory consolidation via Tac2 signaling in mice. *Nat. Commun.* **12**, 2496 (2021).
7. I. Zucker, A. K. Beery, Males still dominate animal studies. *Nature* **465**, 690 (2010).
8. D. A. Bangasser, R. J. Valentino, Sex differences in stress-related psychiatric disorders: Neurobiological perspectives. *Front. Neuroendocrinol.* **35**, 303–319 (2014).
9. R. M. Shansky, Are hormones a "female problem" for animal research? *Science* **364**, 825–826 (2019).
10. R. M. Shansky, A. Z. Murphy, Considering sex as a biological variable will require a global shift in science culture. *Nat. Neurosci.* **24**, 457–464 (2021).
11. D. M. Clark, Anxiety disorders: Why they persist and how to treat them. *Behav. Res. Ther.* **37** (Suppl. 1), S5–27 (1999).
12. A. M. Kaluve, J. T. Le, B. M. Graham, Female rodents are not more variable than male rodents: A meta-analysis of preclinical studies of fear and anxiety. *Neurosci. Biobehav. Rev.* **143**, 104962 (2022).
13. L. Lo, D. J. Anderson, A Cre-dependent, anterograde transsynaptic viral tracer for mapping output pathways of genetically marked neurons. *Neuron* **72**, 938–950 (2011).
14. A. Fujita, L. Zhong, M. S. Antony, E. Chamiec-Case, L. E. Mickelsen, S. E. Kanoski, W. F. Flynn, A. C. Jackson, Neurokinin B-expressing neurons of the central extended amygdala mediate inhibitory synaptic input onto melanin-concentrating hormone neuron subpopulations. *J. Neurosci.* **41**, 9539–9560 (2021).
15. M. A. De Souza Silva, B. Lenz, A. Rotter, T. Biermann, O. Peters, A. Ramirez, F. Jessen, W. Maier, M. Hüll, J. Schröder, L. Frölich, S. Teipel, O. Gruber, J. Kornhuber, J. P. Huston, C. P. Müller, S. Schäble, Neurokinin3 receptor as a target to predict and improve learning and memory in the aged organism. *Proc. Natl. Acad. Sci. U.S.A.* **110**, 15097–15102 (2013).
16. L. R. Glover, K. M. McFadden, M. Bjorni, S. R. Smith, N. G. Rovero, S. Oreizi-Esfahani, T. Yoshida, A. F. Postle, M. Nonaka, L. R. Halladay, A. Holmes, A prefrontal-bed nucleus of the stria terminalis circuit limits fear to uncertain threat. *eLife* **9**, e60812 (2020).
17. B. Bruzsik, L. Biro, D. Zelena, E. Sipos, H. Szebik, K. R. Sarosdi, O. Horvath, I. Farkas, V. Csillag, C. K. Finszter, E. Mikics, M. Toth, Somatostatin neurons of the bed nucleus of stria terminalis enhance associative fear memory consolidation in mice. *J. Neurosci.* **41**, 1982–1995 (2021).
18. K. Asahina, K. Watanabe, B. J. Duistermars, E. Hoopfer, C. R. González, E. A. Eyjólfsdóttir, P. Perona, D. J. Anderson, Tachykinin-expressing neurons control male-specific aggressive arousal in Drosophila. *Cell* **156**, 221–235 (2014).
19. M. Zelikowsky, M. Hui, T. Karigo, A. Choe, B. Yang, M. R. Blanco, K. Beadle, V. Gradinaru, B. E. Deverman, D. J. Anderson, The neuropeptide Tac2 controls a distributed brain state induced by chronic social isolation stress. *Cell* **173**, 1265–1279.e19 (2018).
20. A. P. Wingo, E. R. Velasco, A. Florido, A. Lori, D. C. Choi, T. Jovanovic, K. J. Ressler, R. Andero, Expression of the PPM1F gene is regulated by stress and associated with anxiety and depression. *Biol. Psychiatry* **83**, 284–295 (2018).

21. S. D. Norrholm, T. Jovanovic, B. Vervliet, K. M. Myers, M. Davis, B. O. Rothbaum, E. J. Duncan, Conditioned fear extinction and reinstatement in a human fear-potentiated startle paradigm. *Learn. Mem.* **13**, 681–685 (2006).
22. R. Andero, S. Daniel, J. D. Guo, R. C. Bruner, S. Seth, P. J. Marvar, D. Rainnie, K. J. Ressler, Amygdala-dependent molecular mechanisms of the Tac2 pathway in fear learning. *Neuropsychopharmacology* **41**, 2714–2722 (2016).
23. J. Haaker, S. Gaburro, A. Sah, N. Gartmann, T. B. Lonsdorf, K. Meier, N. Singewald, H. C. Pape, F. Morellini, R. Kalisch, Single dose of L-dopa makes extinction memories context-independent and prevents the return of fear. *Proc. Natl. Acad. Sci. U.S.A.* **110**, E2428–E2436 (2013).
24. Z. Y. Chen, D. Jing, K. G. Bath, A. Ieraci, T. Khan, C. J. Siao, D. G. Herrera, M. Toth, C. Yang, B. S. McEwen, B. L. Hempstead, F. S. Lee, Genetic variant BDNF (Val66Met) polymorphism alters anxiety-related behavior. *Science* **314**, 140–143 (2006).
25. A. W. Fleischer, K. M. Frick, New perspectives on sex differences in learning and memory. *Trends Endocrinol. Metab.* **34**, 526–538 (2023).
26. J. Colom-Lapetina, A. J. Li, T. C. Pelegrina-Perez, R. M. Shansky, Behavioral diversity across classic rodent models is sex-dependent. *Front. Behav. Neurosci.* **13**, 10.3389/fnbeh.2019.00045 (2019).
27. R. Andero, B. G. Dias, K. J. Ressler, A role for Tac2, NkB, and Nk3 receptor in normal and dysregulated fear memory consolidation. *Neuron* **83**, 444–454 (2014).
28. M. Rigby, R. O'Donnell, N. M. J. Rupniak, Species differences in tachykinin receptor distribution: Further evidence that the substance P (NK1) receptor predominates in human brain. *J. Comp. Neurol.* **490**, 335–353 (2005).
29. F. Z. Chung, L. H. Wu, Y. Tian, M. A. Vartanian, H. Lee, J. Bikker, C. Humblet, M. C. Pritchard, J. Raphy, N. Suman-Chauhan, Two classes of structurally different antagonists display similar species preference for the human tachykinin neurokinin3 receptor. *Mol. Pharmacol.* **48**, 711–716 (1995).
30. P. Malherbe, T. M. Ballard, H. Ratni, Tachykinin neurokinin 3 receptor antagonists: A patent review (2005–2010). *Expert Opin. Ther. Pat.* **21**, 637–655 (2011).
31. M. Modi, W. S. Dhillo, Neurokinin 3 receptor antagonism: A novel treatment for menopausal hot flushes. *Neuroendocrinology* **109**, 242–248 (2019).
32. J. A. Harris, K. E. Hirokawa, S. A. Sorensen, H. Gu, M. Mills, L. L. Ng, P. Bohn, M. Mortrud, B. Ouellette, J. Kidney, K. A. Smith, C. Dang, S. Sunkin, A. Bernard, W. Oh, L. Madisen, H. Zeng, *Anatomical characterization of Cre driver mice for neural circuit mapping and manipulation*, *Front. Neural. Circuits.* **8**, 10.3389/fncir.2014.00076 (2014).
33. L. Madisen, T. A. Zwingman, S. M. Sunkin, S. Wook Oh, H. A. Zariwala, H. Gu, L. L. Ng, R. D. Palmiter, M. J. Hawrylycz, A. R. Jones, E. S. Lein, H. Zeng, *A robust and high-throughput Cre reporting and characterization system for the whole mouse brain*, *Nat. Neurosci.* **13**, 133–140 (2010).
34. E. R. Velasco, A. Florido, Á. Flores, E. Senabre, A. Gomez-Gomez, A. Torres, A. Roca, S. Norrholm, E. L. Newman, P. Das, R. A. Ross, A. Lori, O. J. Pozo, K. J. Ressler, L. L. Garcia-Esteve, T. Jovanovic, R. Andero, PACAP-PAC1R modulates fear extinction via the ventromedial hypothalamus. *Nat. Commun* **13**, 4374 (2022).
35. A. Florido, L. Perez-Caballero, E. R. Velasco, P. Molina, I. Marin-Blasco, R. Andero, Direct and indirect measurements of sex hormones in rodents during fear conditioning. *Curr. Protoc.* **1**, e102 (2021).
36. G. M. Raimondi, R. Tripp, L. E. Ostroff, The track-by-day method for monitoring the rodent estrous cycle. *Curr. Protoc.* **3**, e747 (2023).
37. P. Zhou, S. L. Resendez, J. Rodriguez-Romaguera, J. C. Jimenez, S. Q. Neufeld, A. Giovannucci, J. Friedrich, E. A. Pnevmatikakis, G. D. Stuber, R. Hen, M. A. Kheirbek, B. L. Sabatini, R. E. Kass, L. Paninski, Efficient and accurate extraction of in vivo calcium signals from microendoscopic video data. *eLife* **7**, e28728 (2018).
38. G. Paxinos, K. B. J. Franklin, *The Mouse Brain in Stereotaxic Coordinates: Hard Cover Edition*. (Academic Press, 2nd Edition, 2001), 360 pp.
39. M. Famiglietti, F. Leibovici, The impact of health and economic policies on the spread of COVID-19 and economic activity. *Eur. Econ. Rev.* **144**, 104087 (2022).
40. ALFA: Allele Frequency Aggregator; https://ncbi.nlm.nih.gov/snp/docs/gsr/alfa/.
41. A. R. Hariri, A. Tessitore, V. S. Mattay, F. Fera, D. R. Weinberger, The amygdala response to emotional stimuli: A comparison of faces and scenes. *Neuroimage* **17**, 317–323 (2002).
42. D. C. Van Essen, S. M. Smith, D. M. Barch, T. E. J. Behrens, E. Yacoub, *The WU-Minn human connectome project: An overview*, *Neuroimage* **80**, 62–79 (2013).
43. M. F. Glasser, T. S. Coalson, E. C. Robinson, C. D. Hacker, J. Harwell, E. Yacoub, K. Ugurbil, J. Andersson, C. F. Beckmann, M. Jenkinson, S. M. Smith, D. C. Van Essen, A multi-modal parcellation of human cerebral cortex. *Nature* **536**, 171–178 (2016).
44. W. Penny, K. Friston, J. Ashburner, S. Kiebel, T. Nichols, Eds. in *Statistical Parametric Mapping: The Analysis of Functional Brain Images* (Elsevier, 2007); doi: 10.1016/B978-0-12-372560-8.X5000-1.
45. M. Brett, J.-L. Anton, R. Valabregue, J.-B. Poline, Presented at the 8th International Conference on Functional Mapping of the Human Brain. *Japan. Available on CD-ROM in NeuroImage* **16**.
46. V. Baur, J. Hänggi, N. Langer, L. Jäncke, Resting-state functional and structural connectivity within an insula-amygdala route specifically index state and trait anxiety. *Biol. Psychiatry* **73**, 85–92 (2013).
47. S. Torrisi, K. O'Connell, A. Davis, R. Reynolds, N. Balderston, J. L. Fudge, C. Grillon, M. Ernst, Resting state connectivity of the bed nucleus of the stria terminalis at ultra-high field. *Hum. Brain Mapp.* **36**, 4076–4088 (2015).
48. Picture Sequence Memory Test - NIH Toolbox; https://nihtoolbox.org/test/picture-sequence-memory-test/.
49. R. C. Gur, J. D. Ragland, P. J. Moberg, T. H. Turner, W. B. Bilker, C. Kohler, S. J. Siegel, R. E. Gur, Computerized neurocognitive scanning: I. Methodology and validation in healthy people. *Neuropsychopharmacology* **25**, 766–776 (2001).
50. P. D. Zelazo, The Dimensional Change Card Sort (DCCS): A method of assessing executive function in children. *Nat. Protoc.* **1**, 297–301 (2006).
51. B. A. Eriksen, C. W. Eriksen, Effects of noise letters upon the identification of a target letter in a nonsearch task. *Percept. Psychophys.* **16**, 143–149 (1974).
52. W. B. Bilker, J. A. Hansen, C. M. Brensinger, J. Richard, R. E. Gur, R. C. Gur, Development of abbreviated nine-item forms of the Raven's standard progressive matrices test. *Assessment* **19**, 354–369 (2012).
53. Oral Reading Recognition Test - NIH Toolbox; https://nihtoolbox.org/test/a-dummy-iq-test/.
54. Picture Vocabulary Test - NIH Toolbox; https://nihtoolbox.org/test/picture-vocabulary-test/.
55. N. E. Carlozzi, J. L. Beaumont, D. S. Tulsky, R. C. Gershon, The NIH toolbox pattern comparison processing speed test: Normative data. *Arch. Clin. Neuropsychol.* **30**, 359–368 (2015).
56. T. M. Moore, J. C. Scott, S. P. Reise, A. M. Port, C. T. Jackson, K. Ruparel, A. P. Savitt, R. E. Gur, R. C. Gur, Development of an abbreviated form of the Penn Line Orientation Test using large samples and computerized adaptive test simulation. *Psychol. Assess.* **27**, 955–964 (2015).
57. T. M. Achenbach, L. a. Rescorla, Reliability and Validity of ASEBA. *English*, (University of Vermont, Research Center for Children, 2003).
58. T. M. Achenbach, L. Dumenci, L. A. Rescorla, DSM-oriented and empirically based approaches to constructing scales from the same item pools. *J. Clin. Child Adolesc. Psychol.* **32**, 328–340 (2003).
59. K. K. Bucholz, R. Cadoret, C. R. Cloninger, S. H. Dinwiddie, V. M. Hesselbrock, J. I. Nurnberger, T. Reich, I. Schmidt, M. A. Schuckit, *A new, semi-structured psychiatric interview for use in genetic linkage studies: A report on the reliability of the SSAGA*, *J. Stud. Alcohol* **55**, 149–158 (2015).
60. R. R. McCrae, P. T. Costa, JR, Personality in Adulthood. *Personality in Adulthood* (2003); doi: 10.4324/9780203428412.
61. G. Rivero, I. Martín-Guerrero, E. de Prado, A. M. Gabilondo, L. F. Callado, J. A. García-Sevilla, Á. García-Orad, J. J. Meana, *Alpha2C-adrenoceptor Del322-325 polymorphism and risk of psychiatric disorders: Significant association with opiate abuse and dependence*, *World J. Biol. Psychiatry* **17**, 308–315 (2016).
62. J. Sambrook, D. W. Russell, Purification of nucleic acids by extraction with phenol:chloroform. *CSH Protoc.* **2006**, pdb.prot4455 (2006).
63. K. Beckler, State-Trait Anxiety Inventory for Adults Sampler Set Manual, Instrument and Scoring Guide (1983 Consulting Psychologists Press Inc. Mind Garden Inc., 2010), pp. 0–78.
64. A. Spruyt, J. Clarysse, D. Vansteenwegen, F. Baeyens, D. Hermans, Affect 4.0: A free software package for implementing psychological and psychophysiological experiments. *Exp. Psychol.* **57**, 36–45 (2010).
65. T. D. Blumenthal, B. N. Cuthbert, D. L. Filion, S. Hackley, O. V. Lipp, A. van Boxtel, Committee report: Guidelines for human startle eyeblink electromyographic studies. *Psychophysiology* **42**, 1–15 (2005).
66. T. B. Lonsdorf, M. Klingelhöfer-Jens, M. Andreatta, T. Beckers, A. Chalkia, A. Gerlicher, V. L. Jentsch, S. M. Drexler, G. Mertens, J. Richter, R. Sjouwerman, J. Wendt, C. J. Merz, Navigating the garden of forking paths for data exclusions in fear conditioning research. *eLife* **8**, e52465 (2019).
67. T. B. Lonsdorf, M. M. Menz, M. Andreatta, M. A. Fullana, A. Golkar, J. Haaker, I. Heitland, A. Hermann, M. Kuhn, O. Kruse, S. Meir Drexler, A. Meulders, F. Nees, A. Pittig, J. Richter, S. Römer, Y. Shiban, A. Schmitz, B. Straube, B. Vervliet, J. Wendt, J. M. P. Baas, C. J. Merz, Don't fear 'fear conditioning': Methodological considerations for the design and analysis of studies on human fear acquisition, extinction, and return of fear. *Neurosci. Biobehav. Rev.* **77**, 247–285 (2017).
68. R. B. Jain, A recursive version of Grubbs' test for detecting multiple outliers in environmental and chemical data. *Clin. Biochem.* **43**, 1030–1033 (2010).

Acknowledgments: We thank G. Raimondi and L. Ostroff (UConn) for assistance with Track-by-Day estrous cycle tracking. We also thank staff members of the Basque Institute of Legal Medicine for cooperation in the study. We thank Prof. J. Meana for help with the postmortem brain tissue and Dr. M. Fronza for comments on the manuscript. **Funding:** A.F. was a recipient of the Generalitat de Catalunya predoctoral fellowship FI_B00030. E.R.V. was supported by a BES-2017-080870 FPI-2017 fellowship from MINECO. L.R.R. was supported by a PRE2021-099771 fellowship from MINECO. L.P.C. was supported by an FJC2018-037958-I (MCIU). D.P.-C. was supported by a FI19/00251 fellowship from ISCIII. G.R. and E.O. were supported by the Basque Government (IT1512/22). A.N. was a recipient of a predoctoral

fellowship from the Basque Government. T.S. was supported by an NHMRC/MRFF Investigator Grant (MRF1193736), a BBRF Young Investigator Grant, and a University of Melbourne McKenzie Fellowship. M.C. was funded by a Sara Borrell postdoctoral contract (CD20/00189). N.C. was supported by ERANET-Neuron JTC 2019 ISCIII AC19/00088. M.S.A. and A.C.J. are supported by the NIH (R01MH112739 to A.C.J.). R.A. was supported by ERANET-Neuron JTC 2019 ISCIII AC19/00077, Fundacion Koplowitz, RETOS-MINECO PID2020-112705RB-I00 funded by MCIN/AEI/10.13039/501100011033, by "ERDF, A way of making Europe" and MCIN/AEI/10.13039/501100011033, La Caixa HR22-00737, and REIS MCIN/AEI/10.13039/501100011033. R.A.'s work was also produced with the support of a 2022 Leonardo Grant for Researchers and Cultural Creators, and the foundation takes no responsibility for the opinions, statements, and contents of this project, which are entirely the responsibility of its authors. **Author contributions:** A.F. designed the research, performed experiments, analyzed the data and statistics, and wrote the paper. E.R.V. designed the research, performed the research, and analyzed the data. L.R.R., N.A., and I.J.M.B. performed experiments; J.F. analyzed the data; L.P.C. helped with experiments; G.R., E.O., and A.N. performed experiments and analyzed the data; J.A.G.-P. helped with experiments; D.P.-C. and M.C. analyzed the data; T.S. contributed with data and data analysis; M.S.A. performed experiments; N.C. helped with analyses; R.T. helped with experiments; A.C.J. designed the research, performed experiments, and analyzed the data; M.A.F. designed the research and helped with experiments, statistics, data analyses, and interpretation of results. R.A. conceived the study, designed the research, supervised the project, and wrote the paper. All the authors contributed to writing the manuscript. **Competing interests:** R.A. declares a potential conflict of interest with the patent PCT/US2015/037629. The other authors declare that they have no competing interests. **Data and materials availability:** All data needed to evaluate the conclusions in the paper are present in the paper and/or the Supplementary Materials.

Submitted 16 August 2023
Accepted 5 June 2024
Published 10 July 2024
10.1126/sciadv.adk3365